Tracking the Metabolic Signatures Associated with Spinal Muscular Atrophy

Joss Murray

Dr Maria Dimitriadi, Dr George Poulogiannis

May 2018

Submitted to the University of Hertfordshire in partial fulfilment of the requirements of the degree of MSc by Research

Abstract

Spinal muscular atrophy (SMA) is a motor neuron disease and the primary genetic cause of infant death. This disease is caused by the atrophy of motor neurons in the spinal cord resulting in muscle weakness, gradual paralysis and eventual respiratory defects leading to asphyxiation. SMA is characterised by the depletion of the survival motor neuron (SMN) protein – a ubiquitously expressed protein responsible for the regulation of pre-mRNA splicing. The expression of this protein is vital for the development and survival of all tissues, yet, the question still remains as to why SMN depletion affects predominantly motor neurons. Recent developments in SMA research have introduced a multi-organ SMA phenotype, where other tissues affected share a high energy demand. Furthermore, mitochondrial and glucose metabolism defects have been identified in SMA suggesting an energy deficit, which is particularly detrimental to energy-demanding tissues such as motor neurons. In consideration of this, we established a hypothesis stating that all tissues equally suffer an energy deficit as a result of SMN depletion; however the most energy-demanding tissues are affected to the greatest degree. To address this hypothesis, we employed fibroblasts derived from an SMA type I patient and the carrier parents of this individual to identify metabolic alterations putatively generating an energy deficit. The current study proposes a glycolytic and mitochondrial defect in SMA type I patient fibroblasts that is not present in SMA carrier fibroblasts. Furthermore, we identified elevated levels of the metabolite myoinositol, likely stemming from raised inositol monophosphatase (IMPA1) and inositol-3-phosphate synthase (ISYNA1) - a feature shared in SMN knockdown experiments. Considering the relationship between *de novo* myoinositol synthesis and glucose metabolism, we propose that SMN depletion promotes myoinositol synthesis at the cost of energy production from glycolysis. Elevated myoinositol has also been identified in a myriad of other neurodegenerative diseases. Therefore, we propose that myoinositol synthesis may hold potential as a therapeutic target for SMA and other related conditions.

Acknowledgements

First and foremost, I would like to thank my supervisors Dr Maria Dimitriadi and Dr George Poulogiannis for their endless support, wealth of knowledge, and most importantly patience with a developing student. Their combined supervision and tutelage has moulded me into a more confident scientist, and I hope I have made them proud.

The work in this project was performed at the Poulogiannis lab in the Institute of Cancer Research - an establishment that would have been out of reach if not for the opportunity presented by my supervisors. During this project, the entirety of this lab has taken an active interest in my project, and has consistently offered support and opportunities to develop. Drs Amit Gupta, Sara Anjomani-Virmouni, Evi Karali and Adamo Valle always had time for me, whether it was simple advice for an experiment or guiding my professional future. I would also like to thank Marc Turgeon, Nick Perry, Nikos Kondouros, Thanasis Tsalikis, Aurelien Tripp and George Elder, who have been an everlasting fount of support and knowledge throughout this project, and have made many late nights bearable.

I would also like to acknowledge the core facilities at the Institute of Cancer Research for helping with the experiments I could never perform alone. Dr Michel Wagner and Dr Jyoti Choudhary helped performed the liquid chromatography/mass spectrometry experiments, and Radhika Patel and Fredrik Wallberg assisted with the flow cytometry experiments.

Finally, I would like to express my appreciation for my friends and family for their support and encouragement throughout. A hard day was always followed by reassuring words that kept me on track.

Contents

Abbreviations

AGRN – Agrin

ALS – Amyotrophic Lateral Sclerosis

ASO – Antisense Oligonucleotide

ATP – Adenosine Triphosphate

CDK5 – Cyclin Dependant Kinase 5

CM-H2DCFDA – Chloromethyl 2',7'-dichlorodihydrogluorescein Diacetate

CNS – Central Nervous System

ECAR – Extracellular Acidification Rate

ESE – Exon Splice Enhancer

ESS – Exon Splice Silencer

ETC – Electron Transport Chain

FUS – Fused in Sarcoma

GLUT4 – Glucose Transporter Protein 4

GSK3 – Glycogen Synthase Kinase 3

HDAC – Histone Deacetylase

hESC – Human Embryonic Stem Cell

hnRNP1 – Heterogeneous Nuclear Ribonucleoprotein 1

IL6 – Interleukin 6

IMPA1 – Inositol Monophosphatase 1

IP3 – Inositol Triphosphate

iPSC – Induced Pluripotent Stem Cell

ISYNA1 – Inositol-3-Phosphate Synthase 1

LC-MS/MS – Liquid Chromatography-Mass Spectrometry/Mass Spectrometry

mI – Myo-Inositol

MND – Motor Neuron Disease

MRI – Magnetic Resonance Imaging

MRS – Magnetic Resonance Spectroscopy

NCALD – Neurocalcin Delta

NSC-34 – Neuroblastoma/Spinal Cord 34 Cell Line

OCR – Oxygen Consumption Rate

PGK1 – Phosphoglycerate Kinase 1

PI3K – Phophoinositide 3-Kinase

PLS3 – Plastin 3

pre-mRNA – Messenger Ribonucleic Acid Precursor

PTEN – Phosphatase and Tensin Homolog

RIT1 – RAS-like Protein 1

ROCK – Rho-associated Protein Kinase

ROS – Reactive Oxygen Species

shRNA – Short Hairpin Ribonucleic Acid

SLC5A3 – Solute Carrier Family 5 Member 3 (Sodium/Myoinositol Cotransporter)

SMA – Spinal Muscular Atrophy

SMN – Survival Motor Neuron

snRNA – Small Nuclear Ribonucleic Acid

snRNP – Small Nuclear Ribonucleoprotein

SOD1 – Superoxide Dismutase 1

SRSF1 – Serine Arginine Rich Splicing Factor 1

TARDBP – TAR-element DNA Binding Protein

TMRE – Tetramethylrhodamine Ethyl Ester

TNFα – Tumour Necrosis Factor Alpha

VPA – Valproic Acid

YG-box – Tyrosine Glycine-rich Box

ZPR1 – Zinc Finger Protein 1

1. Introduction

1.1 An Overview of Motor Neuron Diseases (MNDs)

Motor neuron diseases (MNDs) encompass a wide range of clinical features involving the gradual loss of motor function due to the death of motor neurons controlling muscles. Diseases within this group include amyotrophic lateral sclerosis (ALS), primary lateral sclerosis (PLS) and spinal muscular atrophy (SMA) (Mitchell & Borasio, 2007; Tiryaki & Horak, 2014). Although MNDs share many symptomatic manifestations, a common mechanistic cause across these diseases has yet to be identified. ALS is the most common MND, however due to the sporadic onset of the large proportion of ALS cases (90%) (Kabashi, et al., 2011), discovering the causative mechanism of this disease and tracking its pathological progression has proven challenging. The remaining 10% of ALS cases are known to be hereditary, yet the wide range of putative genes responsible, such as superoxide dismutase (SOD1), fused in sarcoma (FUS) and TAR DNA-binding protein (TARDBP), and the different molecular pathways they are involved in, act as further confounding factors for the identification of the mechanism/s underlying human disease (Taylor, Brown, & Cleveland, 2017). SMA, however, is caused by a well-defined genetic alteration causing near identical symptoms to ALS. This suggests that identification of a causative mechanism of SMA may likely shed light into identifying the mechanistic basis of other MNDs such as ALS.

SMA is the most common genetic cause of death in children with disease incidence of 1 in 6,000-10,000 (Alías, et al., 2009). Carrier incidences can range between 1 in 35-60, where Caucasian populations hold the highest occurrence (Sugarman, et al., 2012). SMA is of particular interest due to its wide range of severities, the most acute occurring at a very early age. SMA is categorised into four different types according to age of onset and disease severity (Table 1).

Table 1: SMA presents with a range of severities that are characterised clinically by the age of onset and the intensity of symptoms (Wokke, Van Doorn, Hoogendijk, & De Visser, 2013).

SMA Type	Clinical Synonym	Age of Onset	Life Expectancy	Clinical Milestones Reached
I	Werdnig-Hoffman (Acute)	6 Months	2 Years	Unable to sit upright independently, no head control, no ambulation
II	Werdnig-Hoffman (Chronic/Intermediate)	2 Years	10-40 Years	Able to sit upright independently and control head movement, no independent ambulation
III	Kugelberg-Welander (Chronic)	18 Years	Adult	Ambulates independently, likely to require wheelchair assistance by late childhood
IV	Adult-onset	Childhood	Adult	Normal ambulation and movement, mild symptoms aggravate during adulthood

Clinically, SMA is identified by the classic features found in other MNDs such as progressive muscle weakness, gradual paralysis and respiratory defects while mental faculties are left unimpaired (David Arnold, Kassar, & Kissel, 2015). This muscle wastage is due to the early destruction of the alpha

motor neurons found in the anterior horn of the spinal cord (D'Amico, Mercuri, Tiziano, & Bertini, 2011). The resultant loss of innervation of muscle affects motor function, where muscles start to degrade due to decreased workload. Of particular importance is the weakening of masticatory and gastrointestinal muscles important for maintaining nutrition (Messina, et al., 2008), as well as intercostal muscles resulting in respiratory defects as the primary cause of death for severe SMA patients (Chatwin, Bush, & Simonds, 2011). What typically distinguishes SMA from other MNDs like ALS is the early age of onset, range of severities, and most importantly a solitary known genetic cause of disease.

1.2 Spinal Muscular Atrophy: A Single Gene Disorder

Lefebvre et al (1995) identified a common deletion or interruption of an inverted duplication region on chromosome 5q13 in SMA patients and carriers, leading to the discovery of the *SMN* locus, which encompasses the *SMN1* and *SMN2* genes. It was subsequently discovered that (a) patients held homozygous mutations in the telomeric *SMN1*, but not in the centromeric *SMN2* and that (b) both genes produce the ubiquitously expressed SMN protein; however only disruptions in *SMN1* and not SMN2 cause SMA (Coovert, et al., 1997). Monani et al (1999) progressed this work by identifying the difference between *SMN1* and *SMN2* being a single nucleotide polymorphism (SNP; C→T) in exon 7 that controls inclusion of exon 7 into the transcript and final protein product. The cytosine at this position in *SMN1* acts as part of an exon splice enhancer that promotes exon 7 inclusion, while the thymine at the same position in *SMN2* interferes with exon 7 inclusion, resulting in 90% of protein expressed from *SMN2* lacking exon 7 (Figure 1) (Monani, Coovert, & Burghes, 2000; Lorson, Hahnen, Androphy, & Wirth, 1999). The latter is an incomplete and unstable isoform termed SMNΔ7, that gets rapidly degraded; however *SMN2* can still produce full-length SMN protein but in much smaller amounts (10%) compared to *SMN1* (Lunn & Wang, 2008).

Interestingly, it is the *SMN2* copy number that is able to modulate residual SMN levels in order to produce the wide range of SMA severities seen in the clinic (Wirth, et al., 2006), where SMA type I typically presents with 1-2 *SMN2* copies, type II with 2-3 *SMN2* copies, type III with 3-4 *SMN2* copies, and type IV with more than 4 copies of *SMN2* (Butchbach, 2016). Since the full length SMN protein expressed from *SMN2* is identical to the SMN protein expressed from *SMN1*, some effort has been employed for the discovery of drugs that can improve exon 7 inclusion into *SMN2* transcripts under *SMN1* mutation as a therapy for SMA (Mattis, et al., 2006). The antisense oligonucleotide Spinraza (Biogen) is a direct product of this effort displaying very promising efficacy in patients (Scoto, Finkel, Mercuri, & Muntoni, 2017).

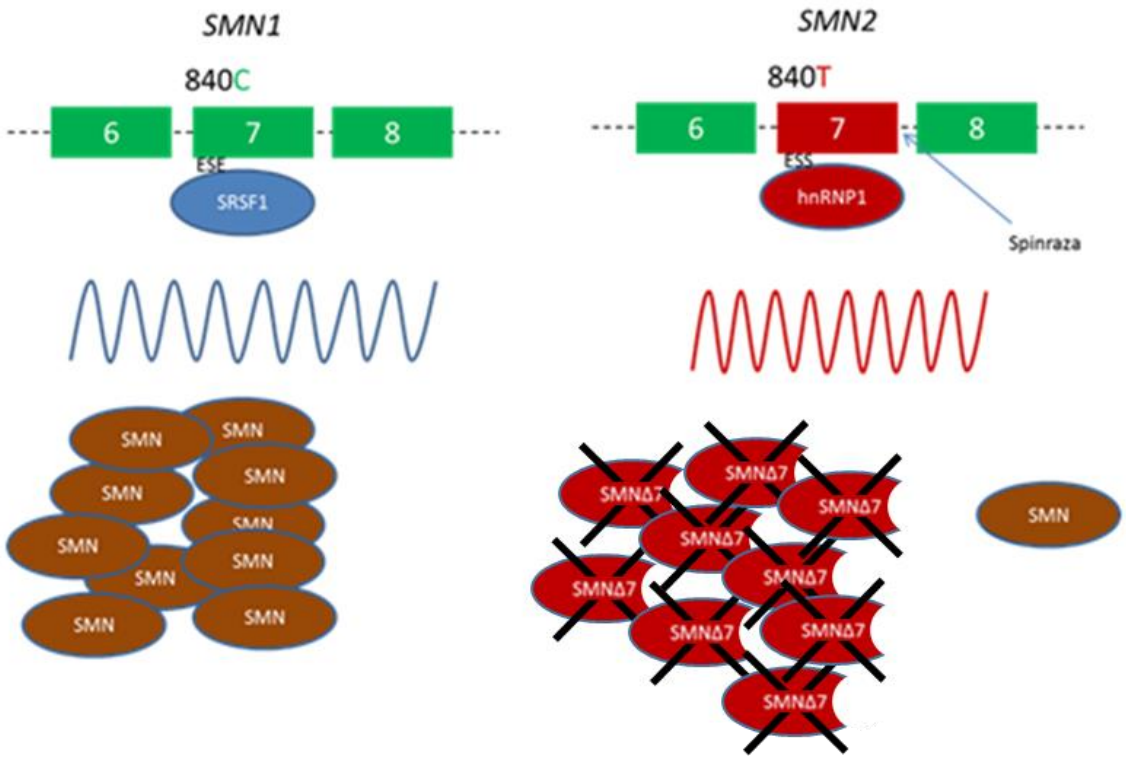

Figure 1: The locus of *SMN1* and *SMN2* on chromosome 5q13. The C→T SNP between *SMN1* and *SMN2*, respectively, interferes with exon 7 inclusion into the mRNA transcript for *SMN2* by converting an exon splice enhancer (ESE) into an exon splice silencer (ESS), thereby dramatically reducing full-length protein production. The antisense oligonucleotide Spinraza binds the intronic sequence ISS-N1 between exon 7 and 8 of *SMN2* to disrupt the binding of negative regulators of exon 7 inclusion, such as hnRNP1 (Dominguez, Cunningham, & Chandler, 2017; Singh, Howell, Androphy, & Singh, 2017).

1.3 The SMN Protein

The SMN protein is ubiquitously expressed across all tissues, raising the important question of why motor neurons are specifically targeted by this deficiency (Monani, 2005). It is thought that although the function of SMN may be vital for all tissues, most can survive with lower levels of expression while motor neurons are particularly susceptible to drops in expression. This hypothesis relies on a protein function of SMN that motor neurons depend on heavily (Burghes & Beattie, 2009), notably its role in the generation of the pre-mRNA splicing machinery.

Structurally, the 294 amino acid long SMN protein is composed of an N-terminal lysine-rich domain, followed by a Tudor domain, a proline-rich domain, and finally a tyrosine-glycine box (YG-box) domain at the C-terminus (Figure 2) (Renviosé, et al., 2006). Glycine zipper conformations are known to be created through oligomerisation between SMN proteins via the C-terminal YG-box, while the Tudor domain is able to recognise methylated arginine residues, typically found in proteins involved in RNA metabolism such as Sm proteins (Martin, Gupta, Ninan, Perry, & Van Duyne, 2012). The ability of SMN to bind RNA metabolism proteins is essential for its principal function in pre-mRNA splicing machinery (Matera & Wang, 2014).

SMN oligomerisation and recruitment of Gemin 2 begins the formation of the SMN complex, a vital machine for small nuclear ribonucleoprotein (snRNP) biogenesis. Recruitment of Gemin 3-8 and Unrip proteins complete the SMN complex, which is now able to facilitate the interactions between Sm proteins and small nuclear ribonucleic acids (snRNAs) to create snRNPs (Rossoll & Bassell, 2009).

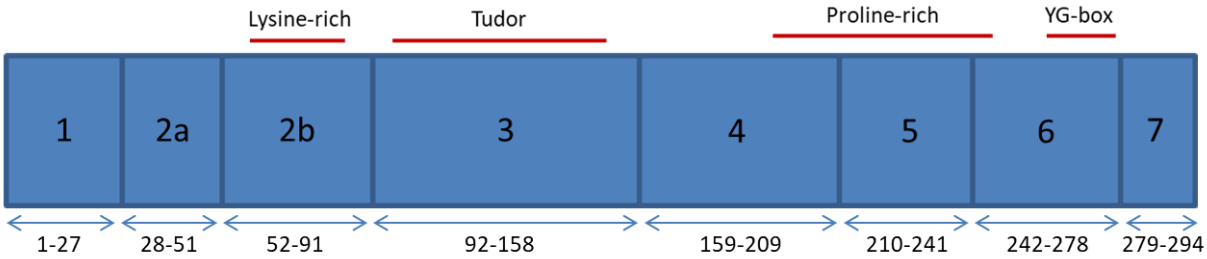

Figure 2: A schematic of the full length SMN coding exons and protein domains. SMNΔ7 is thought to impact SMN oligomerisation by impacting the YG-box, an important primary step for the creation of the SMN complex. Exon 8 is untranslated (Renviosé, et al., 2006; Rossoll & Bassell, 2009).

The snRNPs are responsible for the removal of introns in pre-mRNA in order to control the alternative splicing and maturation of mRNA transcripts (Singh & Cooper, 2012). This subsequent regulation of splicing is thought to be the primary, canonical function of SMN. Therefore SMN deficiency is thought to induce errors in splicing due to faulty snRNP biogenesis, where a correlation between SMN-dependant snRNP assembly and SMA severity has been drawn (Burghes & Beattie, 2009). However, why depletion of a ubiquitously expressed protein resulting in damage to a ubiquitous cellular process is detrimental to specifically and solely motor neurons is unknown.

One solution to this conundrum lies in the preference of SMN depletion to impair production of snRNP species that compose the minor spliceosome, as evident in mouse models of SMA (Gabanella, et al., 2007). The minor spliceosome is responsible for regulating the splicing of transcripts containing U12 introns, which account for less than 0.5% of all introns in the genome (Turunen, Niemelä, Verma, & Frilander, 2013). This implies that faulty splicing of U12 introns may play a large part in SMA pathogenesis, where genes that motor neurons rely on may possess a higher occurrence of containing U12 introns. The gene *Stasimon*, for example, has been identified in *Drosophila* and zebrafish models as a gene containing a U12 intron, which under SMN depletion is aberrantly spliced ultimately resulting in a reduction of Stasimon protein expression (Lotti, et al., 2012). Stasimon is a transmembrane protein vital for motor neuronal synaptic homeostasis, and depletion of this protein alone displays a phenotype similar to SMA in *Drosophila* models (Boulisfane, et al., 2010). Interestingly, expression and splicing of the murine homolog of *Stasimon* – *Tmem41b* – was found to be unaltered in an SMA mouse model (Zhang, et al., 2013), suggesting that mis-splicing of *Stasimon* may not translate in SMA patients. Nevertheless, *Stasimon* is an example of a gene containing a U12 intron, and therefore promise still lies in examining other genes with U12 introns for altered expression under SMN depletion that may be responsible for selective motor neuron vulnerability in SMA. However, many groups have turned to identifying non-canonical functions of SMN that may lead to motor neuron vulnerabilities while sparing other tissues (Zhang, et al., 2006; Fallini, Bassell, & Rossoll, 2012; Garcera, Bahi, Peiyakaruppiah, Arumugam, & Soler, 2013; Gabanella, et al., 2016; Singh, Howell, Ottesen, & Singh, 2017).

1.4 Other Functions of SMN

The SMN protein localises to the nuclear gems in order to perform its canonical function of snRNP biogenesis (Clelland, Kinnear, Oram, Burza, & Sleeman, 2009), however the SMN protein has also been reported in the cytoplasm (MacKenzie & Gendron, 2001). This cytoplasmic localisation is in part due to the recruitment of Gemins to form the SMN complex in order to begin snRNP biogenesis (Beattie & Kolb, 2018). The ability of SMN to shuttle between the nucleus and the cytoplasm has also been shown to be important for the transport of mRNAs across the cell, of particular importance for long cells such as neurons (Fallini, Bassell, & Rossoll, 2012). For example, SMN has been shown to interact with β-actin mRNA to aid its expression across neurons (Zhang, et al., 2003), which is thought to promote the maturation of neuronal axons (Rossoll, et al., 2003). This transport of mRNA likely impacts the formation of stress granules – cellular reservoirs of proteins and mRNAs to be released under stress conditions (Potter & Parker, 2016); where depletion of SMN has also been shown to impair the ability of stress granules formation (Zou, et al., 2011). SMN has also been implicated to further regulate gene expression through interactions with transcriptional proteins such as RNA polymerase II (Pellizzoni, Charroux, Rappsilber, Mann, & Dreyfuss, 2001), p53 (Young, et al., 2002) and Sin3A (Zou, et al., 2004).

Additionally, SMN deficiency gives rise to defects in endocytosis (Dimitriadi, et al., 2016; Reissland, et al., 2017), introducing a neuronal-specific function of SMN through synaptic vesicle control. While mis-splicing of endocytic genes may be responsible for this defect, a possible interaction between SMN and the cytoskeleton presents an alternative explanation (Nash, et al., 2017). For example, SMN has been shown to control actin polymerisation and to interact with cytoskeletal proteins Profilin I/II (Bowerman, Shafey, & Kothary, 2007), therefore reinforcing the possibility that endocytic defects may arise through altered cytoskeletal integrity in SMA (Bowerman, et al., 2009). Furthermore, autophagic markers have been shown to be elevated in murine SMA motor neurons (Garcera, Bahi, Peiyakaruppiah, Arumugam, & Soler, 2013), implying that SMN may regulate autophagy. This feature has been explored further, where autophagy inhibitors have displayed efficacy in improving SMA symptoms in mouse models (Piras, et al., 2017). This myriad of secondary functions of SMN emphasises the range of potential therapeutic targets for SMA.

1.5 Genetic Modifiers of SMA

Considering the multitude of secondary functions of SMN, it stands to reason that a variety of pathways can be altered to improve SMA symptoms. This gives rise to a wide range of genetic components that can putatively alter the SMA phenotype. As previously discussed, a powerful genetic modifier of SMA severity is *SMN2*, where a positive correlation exists between *SMN2* copy number and SMA severity (Prior, et al., 2009). To this end, eight copies of *SMN2* have been reported to fully rescue the SMA phenotype in mice (Monani, et al., 2000). A number of other SMA genetic modifiers have been reported in experimental models; however two genetic modifiers have been identified in individuals expressing low SMN protein while remaining asymptomatic (Table 2): *PLS3* and *NCALD*.

PLS3 encodes the protein Plastin 3, a SMN-associated actin bundling protein that was found to be overexpressed in eight asymptomatic females with the same *SMN1* and *SMN2* genotypes as their SMA affected siblings (Oprea, et al., 2008). Interestingly, Plastin 3 is a gender specific genetic

modifier of SMA severity since the locus of *PLS3* is on chromosome X (Stratigopoulos, et al., 2010). Further assessment of *PLS3* as a genetic modifier of SMA severity has revealed that overexpression of *PLS3* in a mouse model of intermediate SMA can improve symptoms and survival by increasing F-actin levels necessary for axonogenesis (Oprea, et al., 2008). Furthermore, *PLS3* overexpression enhances the efficacy of a splice switching antisense oligonucleotide therapy (ASO) that increases SMN protein production from *SMN2* (Kaifer, et al., 2017). Considering that Plastin 3, Profilin and β-actin have been implicated in SMA pathogenesis (Bowerman, et al., 2009), and that endocytic vesicle trafficking is also defective in SMA (Dimitriadi, et al., 2016), cytoskeleton dynamics hold potential as an effective therapeutic target for the treatment of SMA. Employing this rationale, application of an inhibitor of the RhoA/Rho kinase (ROCK) pathway, a major regulator of the cytoskeleton (Amano, Nakayama, & Kaibuchi, 2010), has shown promising improvement to the SMA phenotype in mice (Bowerman, Murray, Boyer, Anderson, & Kothary, 2012).

NCALD encodes the protein Neurocalcin Delta, a neuronal calcium sensor protein, which was found to be under-expressed in five asymptomatic individuals carrying homozygous *SMN1* mutations and four *SMN2* copies (Reissland, et al., 2017). Neurocalcin Delta is able to interact with the cytoskeletal proteins tubulin and actin, as well as clathrin, which is vital for endocytosis (Kaksonen & Roux, 2018; Ivings, Pennington, Jenkins, Weiss, & Buroyne, 2002). Combined with Plastin 3, this emphasises a cytoskeletal and endosomal trafficking role in SMA pathogenesis. Interestingly, another commonality between Plastin 3 and Neurocalcin Delta is their role in calcium signalling. Both of these proteins possess calcium binding EF hand domains, and therefore calcium is vital for these proteins to regulate their functions (Lyon, et al., 2014; Ivings, Pennington, Jenkins, Weiss, & Buroyne, 2002). Considering that abnormal calcium signalling has been reported as a feature of SMA (Jablonka, Beck, Lechner, Mayer, & Sendtner, 2007; McGivern, et al., 2013), and that healthy calcium signalling is important for both neuronal cytoskeletal homeostasis (Heimfarth, et al., 2016) and clathrin-mediated endocytosis (Santos, et al., 2017), it seems likely that *PLS3* and *NCALD* act as genetic modifiers of SMA through calcium homeostasis and subsequent regulation of endocytosis and the cytoskeleton.

Besides *PLS3* and *NCALD*, various other genes have been reported to modify disease severity under altered expression in experimental models (Table 2). Interestingly, these genetic modifiers are implicated in a wide variety of molecular functions, emphasising the multitude of possible pathways influenced by SMN. While this makes the identification of a definitive pathogenic function of SMN in SMA difficult, it could open many novel opportunities for therapy.

Table 2: A variety of genes have been reported to modify SMA severity (Hosseinibarkooie, Schneider, & Wirth, 2017). *SMN2*, *PLS3* and *NCALD* have been identified as genetic modifiers of SMA in patients, while *PTEN*, *ZPR1*, *AGRN* and *PGK1* were identified as potential modifiers of SMA through experimental evidence in model organisms.

Gene Name	Protein Name	Function	Condition to Improve SMA	Reference
SMN2	Survival Motor Neuron	RNA processing, assembly of splicing machinery	Over expression	Gavrilov, et al., 1998
PLS3	Plastin 3	Actin bundling protein	Over expression	Oprea, et al., 2008
NCALD	Neurocalcin Delta	Neuronal calcium sensor regulating endocytosis	Under expression	Riessland, et al., 2017
PTEN	Phosphatase and Tensin Homology	Negative regulator of PI3K-AKT signalling	Under expression	Little, et al., 2015
ZPR1	Zinc Finger Protein 1	Interacts with SMN to facilitate interactions with mRNA	Over expression	Ahmad, et al., 2012
AGRN	Agrin	Proteoglycan responsible for NMJ development	Over expression	Boido, et al., 2018
PGK1	Phosphoglycerate Kinase 1	Glycolytic enzyme	Over expression	Boyd, et al., 2017

1.6 Therapeutic Strategies for SMA

The majority of SMA therapeutic efforts are aiming at improving endogenous SMN protein expression since SMA is characterised by the depletion of a single protein. As reviewed by d'Ydewalle and Sumner (2015), these current pipeline therapies can be broken into four main groups: (a) *SMN2* promoter activation (RG3039), (b) *SMN2* splicing modulation (Spinraza), (c) *SMN1* replacement therapy (AVXS-101) and (d) neuroprotective therapy (Olesoxime). *SMN2* gene expression modulators such as the compound RG3039 rely on enhancing *SMN2* expression through promoter interactions, therefore increasing the amount of full length SMN protein being expressed. Unfortunately, promising progress on this compound has been halted after the collaborative effort between Repligen and Pfizer ended (Kaczmarek, Schneider, Wirth, & Riessland, 2015). Besides the success of Spinraza so far, the AveXis *SMN1* gene replacement therapy AVXS-101 has shown promise in a recent clinical trial where all SMA type I patients receiving a dose of adeno-associated virus carrying SMN cDNA were alive and event free by 20 months of age (Mendell, et al., 2017). In addition, Olesoxime is a neuroprotective agent shown to improve symptoms of a range of neurodegenerative conditions. This compound achieves its mechanism of action through mitochondrial interactions to improve energy production and reduce the release of mitochondrial pro-apoptotic factors (Bertini, et al., 2017). Olesoxime is an example of a small group of drugs that aim to improve patient outcome without targeting SMN levels. The rationale for the emergence of this class of therapy is due to the hypothesis that SMN is important for motor neuron development during the embryonic and post-natal stages, rather than the post-mitotic maintenance stage (Gabanella, Sarissimi, Usiello, & Pellizzoni, 2005). This suggests that some patients may not benefit

from augmenting SMN levels and would better tolerate a therapy targeting the maintenance of healthy motor circuits. While Olesoxime has shown patient improvement in milder type II and III SMA, it has been concluded that perhaps this neuroprotective agent may prove most beneficial to patients in combination with other similar therapies (Bertini, et al., 2017).

The development of Spinraza has introduced the field of ASO therapies, which presents advantageous opportunities for various other diseases. However, without the development of competing SMA therapies, treatments may remain inaccessible to the vast majority of families affected. Furthermore, the identification of compounds that may benefit other diseases similar to SMA can introduce novel therapeutic routes as well as the possibility of combination therapy for improved efficacy. Examples of this include the suggested value of the ALS therapy riluzole in SMA (Orrell, 2010; Dimitriadi, Kye, Kalloo, Yersak, & Hart, 2013). Pharmaceutical novelty, however, requires the identification of innovative differences between healthy and disease state that turns out to be advantageous for symptomatic improvement.

1.7 Advent of –omics Techniques to Guide Innovation in SMA Treatment

The growing popularity in –omics techniques has introduced high-throughput methods of identifying alterations between samples. This has unveiled many putative targets for therapy in a number of different diseases, with MNDs being no exception.

Of particular interest in SMA, considering the implied dysfunction of splicing machinery, is the utilisation of transcriptomic techniques to identify alternative splicing events in the disease state to unveil proteomic targets. This route has proven successful in identifying upregulation of *TNFα* and *IL6*, among others (in a mouse model of severe SMA), both known to control neural and cardiac development (Yang, et al., 2016). Transcriptomic analysis of SMN knockdown in the motor neuron-like NSC-34 cell line displayed a variety of splicing defects, namely intron retention in transcripts from *RIT1* – which when over expressed in this model was able to restore neurite defects (Custer, et al., 2016). RNA sequencing of multiple tissues from a mouse model of SMA type III has identified U12 intron retention across all tissues, resulting in mis-splicing of multiple calcium homeostasis genes as well as *CDK5*: a kinase known to be important for neural development that is known to be deregulated in multiple other neurodegenerative diseases (Doktor, et al., 2017).

Epigenetic modulation has been proposed as an effective therapeutic route for SMA, where modifying the epigenome is thought to improve the expression of *SMN2,* subsequently improving the levels of SMN protein. The main target for this epigenomic therapeutic approach was through interactions with histone deacetylases (HDAC), where HDAC inhibitors such as sodium butyrate and valproic acid were shown to improve *SMN2* transcription in cell culture and mouse models, albeit with limited clinical efficacy in patients (Chang, et al., 2001; Brichta, et al., 2003; Sumner, et al., 2003; Chuang, Y., Marinova, Kim, & Chiu, 2009; Tisdale & Pellizzoni, 2015).

Interestingly, little has been achieved with identifying metabolomic targets in SMA (Farrar, et al., 2017). This approach is of particular importance as forming a fingerprint that separates SMA from healthy states can reveal pathways that may otherwise have little genomic, transcriptomic or proteomic differences.

Glucose metabolism alterations have been identified in SMA patients and mouse models as a result of cellular remodelling of the pancreatic islets, where glucagon-producing α cells increase at the cost of insulin-producing β cells (Bowerman, et al., 2012; Bowerman, et al., 2014). The resulting lack of insulin is the likely cause of the impaired glucose tolerance observed in patients (Davis, Miller, Zhang, & Swoboda, 2015). Metabolic disorders are a common consideration for SMA patients due to lack of exercise, however it has been acknowledged that glucose metabolism defects may be intrinsic to the disease resulting in the recommendation to monitor glucose levels in SMA patients (Mercuri, et al., 2018). The downstream implications for altered glucose metabolism in SMA, however, have yet to be explored.

Mitochondrial abnormalities have also been well described in SMA, implying that an energy deficit may be, at least in part, responsible for SMA disease progression (Ascadi G. , et al., 2009; Miller, Shi, Zelikovich, & Ma, 2016; Xu, Denton, Wang, Zhang, & Li, 2016). These defects, summarised in Table 3, ultimately illustrate deficient ATP synthesis from mitochondria that can contribute to a damaged energetic state in SMA. This concept supports the SMA phenotype of selective motor neuron degeneration, where motor neurons have been described to have a high energy demand, and therefore damaged ATP synthesis will preferentially affect motor neurons over other tissues (Le Masson, Przedborski, & Abbott, 2014; Malkki, 2016; Perera & Turner, 2016). Additionally, glucose metabolism defects could further lower ATP production from glycolysis emphasising the potential energy deficit in SMA motor neurons.

Further evidence of metabolic alterations in SMA stems from examining effects of SMN depletion on other tissues besides those of the nervous system. Cardiac defects have been noted in both severe SMA patients (Rudnik-Schöneborn, et al., 2008) and mouse models (Bevan, et al., 2010) ranging from structural to rhythmic abnormalities. Liver defects have also been reported, where depletion of SMN in the liver was shown to induce errors in iron homeostasis and embryonic hepatic development (Vitte, et al., 2004). Combined with known pancreatic defects in SMA, these data introduce a multi-organ phenotype in SMA with a metabolic phenotype theme, where the organs affected in the disease either have a high metabolic demand, or a high metabolic contribution (Himilton & Gillingwater, 2013).

Table 3: Studies reporting metabolic defects in SMA. The studies range from clinical findings to experimental discoveries in mouse, zebrafish and 2D cell culture models. Of these findings, glucose metabolism abnormalities and mitochondrial dysfunction are common between models of SMA.

Authors	SMA Model	Main Findings
Crawford, et al., 1999	Patients with severe infantile SMA	Altered fatty acid profile in patients compared to other denervating disorders; disease severity correlated with incidence of diacarboxylic aciduria
Berger, et al., 2003	Muscle biopsies from patients with SMA type I-III	Decrease in mitochondrial DNA relative to nuclear DNA; reduction in electron transport chain complex II activity and cytochrome *c* oxidase
Ascadi, et al., 2009	SMN knockdown in NSC-34 motor neuron-like cells	Reduced ATP levels, increased mitochondrial membrane potential, increased ROS levels, altered activity of oxidative phosphorylation enzyme Cytochrome *c* Oxidase
Butchbach, et al., 2010	SMNΔ7 SMA mice fed with two different diets differing in fat content	SMA mice fed a higher fat diet was found to survive longer than mice fed the lower fat diet
Bowerman, et al., 2012	Intermediate SMA mouse model, type I SMA patients	Pancreatic cellular remodelling (increase α cells and decrease β cells), hyperglycaemia, hyperglucagonemia, glucose resistance
Bowerman, et al., 2014	Heterozygous SMN depletion mouse model, seemingly healthy at 1 month	Introduction to high fat diet induces pancreatic cell remodelling, increased hepatic insulin, elevated glucagon sensitivity; suggests SMA carriers at risk of metabolic disorders
Davis, et al., 2015	Patients with SMA type II	Impaired glucose tolerance, hyperinsulinemia, insulin resistance, elevated free fatty acid levels and reduced plasma amino acids are common features between many participants
Ripolone, et al., 2015	Quadricep muscle biopsies from patients with SMA type I-III	Cytochrome *c* Oxidase deficiency and reduced activity of electron transport chain complexes I, II and IV were more evident in severe SMA phenotypes
Miller, et al., 2016	Motor neurons sourced from an SMA mouse model	Altered expression of mitochondrial bioenergetics genes, reduced basal and maximal mitochondrial respiration, increases oxidative stress, damaged mitochondrial membrane potential, impaired mitochondrial transport, increased mitochondrial fragmentation during presymptomatic stage of SMA
Xu, et al., 2016	Motor neurons derived from SMA type I iPSCs, SMN knockdown in motor neurons derived from hESCs	Reduction in mitochondrial number, area and transport in axons of both models; application of *N*-acetylcysteine (antioxidant) ameliorates mitochondrial defects
Boyd, et al., 2017	Severe SMA mouse model, morpholino knockdown of SMN in zebrafish	Bioenergetic gene expression in motor neuron populations dictates vulnerability to SMA progression; enhancing mitochondrial biogenesis and over expressing phosphoglycerate kinase improves motor axon defects in SMA zebrafish
Kölbel, et al., 2017	Patients with SMA type I-III	Hyperleptinemia significantly associated with SMA severity and motor function; elevated leptin levels prevalent in underweight children with SMA

1.8 Project Aims

Considering the abnormal mitochondria and mounting evidence of glucose metabolism defects in SMA (Table 3), we hypothesise that metabolic alterations in patients may be a result of SMN depletion that preferentially affects highly energetic tissues such as motor neurons and muscle. The work in this thesis focuses on delineating the metabolic defects in SMA, with the ultimate goal to identify novel metabolic alterations in SMA that may be exploitable for novel therapeutic interventions. To address this, we utilised fibroblasts derived from an SMA type I patient, and fibroblasts derived from the two SMA carrier parents of this individual.

In this study, we aimed to build on current data of an aberrant metabolic environment in SMA by identifying alterations in energetic profiles using Agilent Biosciences Seahorse Extracellular Flux technologies to measure glycolytic and mitochondrial function. We also utilised fluorometric techniques to further describe mitochondrial defects present in these SMA fibroblasts. Finally, metabolomic analysis using liquid chromatography-mass spectrometry (LC-MS/MS) was employed to identify variances in metabolite profiles between SMA affected and carrier fibroblasts (Figure 3). This work is intended to contribute to the growing evidence of metabolic dysfunction in SMA and other MNDs and introduce metabolism as a novel potential target for the treatment of this devastating disease.

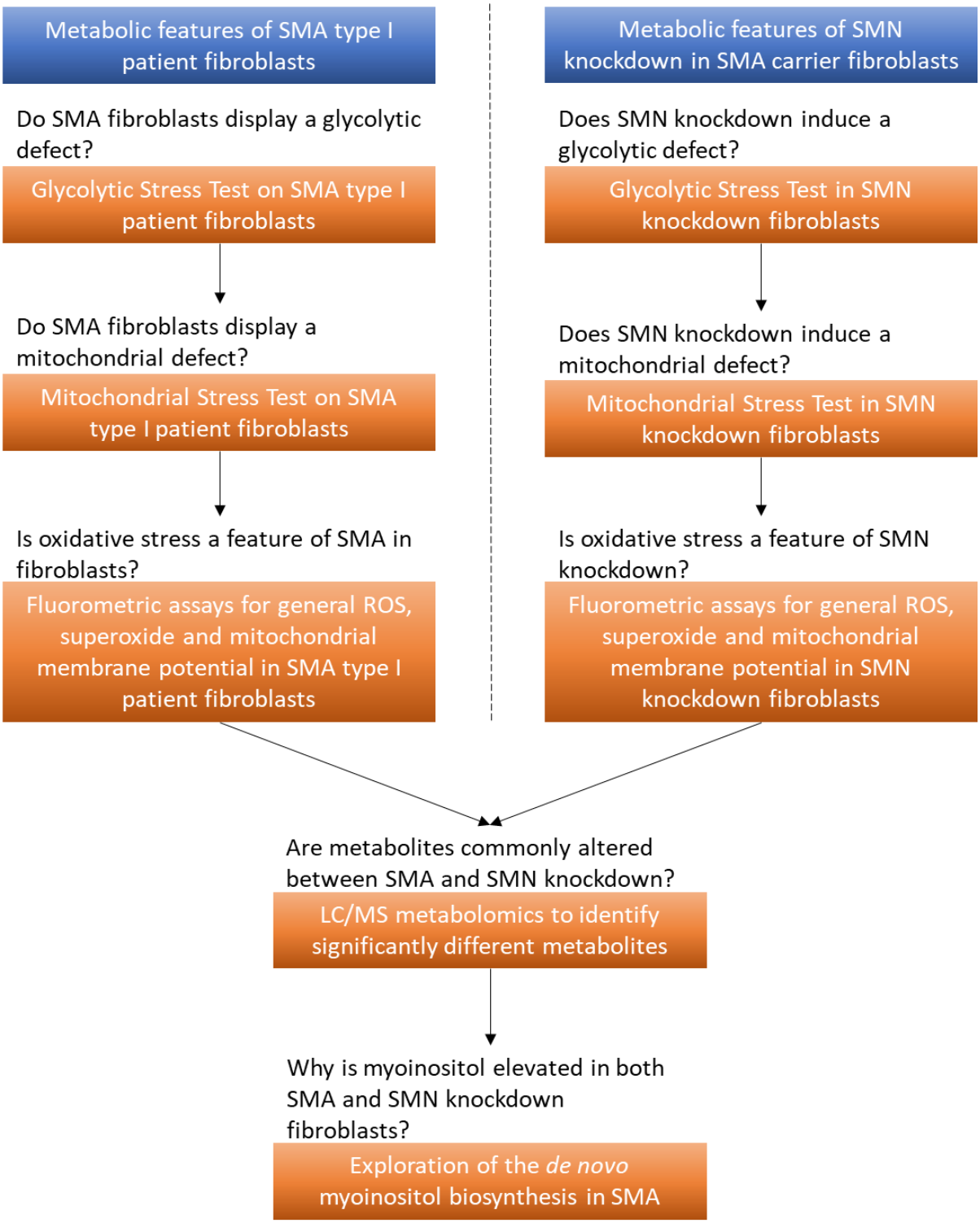

Figure 3: The biological questions asked in the current proposal and the experimental procedures used to address them. In this thesis, we aimed to address whether SMA fibroblasts demonstrate glycolytic, mitochondrial and/or oxidative stress defects, and to identify putative metabolites associated with SMN depletion.

2. Methods

2.1 Cell Culture

Fibroblasts were sourced from Coriell Cell Repository (Camden, NJ, USA) (Table 4). Since different tissues vary in their metabolic profile (Shlomi, Cabili, Herrgård, Palsson, & Ruppin, 2008), GM03813, GM03814 and GM03815 were chosen for the experiments described here due to their consistent tissue type and biopsy source. Furthermore, these fibroblasts are sourced from individuals within a family; therefore some degree of genetic control can be maintained within these three cell lines.

Table 4: Fibroblasts obtained from the Coriell Cell Repository that were used in this study. General information and characteristics of the fibroblast cell lines based on the Coriell Cell Repository webpages. SMN2 copy number information obtained from Stabley et al, 2017.

Cell Line Number	Coriell Description	Affected	Gender	Age	Biopsy Source	Cell type	Tissue Type	*SMN2* Copy Number
GM03813	SPINAL MUSCULAR ATROPHY I; SMA1	YES	MALE	3 Years	Arm	Fibroblast	Skin	3
GM03814	SPINAL MUSCULAR ATROPHY I; SMA1	NO	FEMALE	N/A	Arm	Fibroblast	Skin	5
GM03815	SPINAL MUSCULAR ATROPHY I; SMA1	NO	MALE	N/A	Arm	Fibroblast	Skin	1

Fibroblasts were cultured in Dulbecco's Minimum Essential Medium (DMEM) supplemented with 15% fetal bovine serum (FBS) (Gibco Lot no. 20470), 100U/mL penicillin and 100ug/mL streptomycin. Cells were grown at 37°C in a humidified incubator with 5% (vol/vol) CO_2. Fibroblasts transfected with SMN shRNAs were cultured in DMEM supplemented with 15% FBS, the aforementioned antibiotics and 2 µg/mL puromycin (Invivogen). Sub-culturing required brief washing of attached cells with phosphate buffered saline (PBS) followed by incubation with 0.05% trypsin in 0.02% Versene for 5-15 minutes to detach cells. Following detachment, cells were collected and centrifuged at 180 x g to remove trypsin, and reseeded as necessary.

Fibroblasts were cryopreserved by re-suspending cell pellets in FBS supplemented with 10% dimethyl sulphoxide (DMSO) and aliquoting into 1.5 mL cryotubes. Tubes were incubated in a Mr. Frosty Freezing Container (Nalgene) at -80°C for 24-72 hours before transfer into liquid nitrogen for long term storage. Cells were thawed by briefly incubating cryotubes in a water bath at 37°C before mixing cells with fresh medium. This mixture was centrifuged in order to aspirate DMSO, followed by re-suspending the resulting cell pellet in fresh medium and seeding on a 10 cm^2 plate. Medium was changed the morning after thawing cells to ensure any residual DMSO was removed.

2.2 SMN Knockdown shRNA Preparation

Lentiviral short hairpin RNAs (shRNAs) targeting SMN transcripts were sourced from the Dharmacon RNAi Consortium. Five shRNAs targeting SMN were available from this collection, designated clone IDs TRCN0000118702-TRCN0000118706. For the experiments proposed herein, these hairpins were renamed shSMNa-shSMNe, respectively. The shRNA constructs are conjugated into the pLKO.1 vector, therefore a pLKO.1 shGFP construct was used as a negative control for SMN knockdown.

Each construct was transformed into MAX Efficiency DH5α Competent cells (Thermo) by the heat shock method. 200 ng of each construct was added to aliquots of DH5α cells followed by flicking gently and incubation on ice for 30 minutes. Cells were then subjected to heat shock in a 42°C water bath for 45 seconds, followed by incubation on ice for 2 minutes. 250 µL of super optimal broth with catabolite repression (S.O.C medium – 2% tryptone, 0.5% yeast extract, 20 mM glucose, 10 mM sodium chloride, 2.5 mM potassium chloride, 10 mM magnesium chloride, 10 mM magnesium sulphate – Thermo) was added to each tube to aid recovery after heat shock. Cells were incubated for 60 minutes at 37°C and pipetted onto agar plates containing ampicillin before getting spread across the plates evenly. Plates were incubated at 37°C overnight. A colony from each plate was picked and dropped into a 2 L Erlenmeyer flask with 250 mL LB broth supplemented with ampicillin. Flasks were placed in a shaking incubator overnight at 37°C.

Bacterial suspension cultures were poured into centrifuge bottles and pelleted at 2,160 x g at 4°C for 10 minutes. Pellets were re-suspended in 5mL of cold alkaline lysis solution I (50 mM glucose, 25 mM Tris pH 8, 10 mM EDTA pH 8 in filtered water) and transferred to a 50 mL tube, followed by addition of 25 mg lysozyme and incubation at room temperature for 8 minutes. 10 mL of freshly made solution II (200 mM sodium hydroxide and 4% SDS in filtered water) was added and incubated on ice for 10 minutes with regular agitation. 7.5 mL of solution III (3 M potassium acetate and 115 mM glacial acetic acid in filtered water) was then added and incubated on ice for a further 10 minutes. Tubes were then centrifuged at 13,500 x g at 4°C for 20 minutes. The supernatant was then discarded and the pellets were air dried for 10 minutes. Once dry, pellets were re-suspended in 4 mL TE pH 8 buffer (10 mM Tris pH 8 and 1 mM EDTA pH 8 in filtered water), followed by 2 mL of 7.5 M cold ammonium acetate and incubation on ice for 30 minutes. Tubes were then centrifuged for a further 10 minutes at 4°C at 9,400 x g. The supernatant was then transferred to a fresh tube, and 12 mL of cold ethanol was added and incubated overnight at -20°C.

Tubes were centrifuged at 9,400 x g for 10 minutes at 4°C, the resulting supernatant was discarded, and the pellet was left to air dry for 10 minutes. 500 µL of TE pH 8 buffer was used to re-suspend the pellets, which was then transferred to a fresh microtube. 1 µL of 10 mg/mL RNase was added to each tube and incubated at 37°C for 30 minutes, followed by phenol-chloroform extractions. 250 µL cold phenol and 250 µL chloroform was added to each tube and vortexed, followed by centrifuging at max speed at room temperature for 5 minutes. The aqueous phase from this tube was transferred to a fresh, microtube followed by two further additions of chloroform extractions, pooling each aqueous phase into the same tube, followed by addition of 50 µL 3 M sodium acetate. 1 mL of cold ethanol was added to each tube followed by spooling the resulting DNA, which was transferred to a fresh microtube containing 70% ethanol. Tubes were centrifuged at max speed at 4°C for 5 minutes, followed by removal of the supernatant and air drying. Dried DNA pellet were re-suspended with 50 µL of TE and quantified using a ND-1000 Spectrophotometer (Nanodrop).

2.3 Transfection and Transduction of SMN shRNAs

Transfection of shRNA constructs required composing a mixture of the shRNA and lentiviral packaging vectors. Quantities of each component used are as follows: 0.4ug SVG, 3.7ug GAG, 3.7ug REV, 4.2ug shRNA construct. Each mixture was made up to 20uL with PCR grade water. Once these DNA mixtures were composed for each shRNA construct, mixtures of 556 µL of room temperature serum-free DMEM and 24 µL FuGENE HD Transfection Reagent (Promega) were prepared for each DNA mixture. To this, the 20 µL DNA mixture was added for a total transfection mixture of 600uL. These transfection mixtures were left to stand at room temperature for 30 minutes. During this

time, the medium of 50% confluent HEK293T seeded in 10cm^2 plates that were plated the previous day was aspirated and replaced with 6mL of fresh DMEM supplemented with 10% FBS. After the 30 minute incubation, the 600 µL transfection mixtures were added to HEK293T cells dropwise and incubated in a humidified 37°C incubator with 5% (vol/vol) CO_2 for 6 hours. The medium was then removed and replaced with 10 mL fresh DMEM supplemented with 10% FBS and left to propagate lentiviral particles for 48 hours. The viral medium was then harvested using a syringe with a 19½ gauge needle, and filtered into 1 mL microtube aliquots. These tubes were stored at -80°C for future use.

In preparation for the infection of GM03814 cells, 200,000 cells were seeded per well for each shRNA in a 6 well plate. The day after seeding fibroblasts were cultured in 2ml lentiviral-containing medium with 4 µg/mL polybrene, and incubated for 24 hours at 37°C. Medium was then replaced with fresh DMEM supplemented with 15% FBS for 24 hours to allow the cells to recover from infection. Finally, selection began using DMEM supplemented with 15% FBS and 2 µg/mL puromycin which was changed every 2-3 days. Knockdown cells were maintained in puromycin medium for the experiments described herein.

2.4 Western Blotting

Plates of 70-80% confluent cells were washed with cold PBS and snap frozen in liquid nitrogen. Lysis buffer composed of RIPA Lysis and Extraction Buffer (Thermo) supplemented with 1 µg/mL pepstatin A (Sigma), 1 µg/mL leupeptin (Sigma), 250 µM β-glycerophosphate (Sigma), 2 mM sodium orthovanoate (Sigma), 1 mM dithiothreitol (Sigma), 10 mM calyculin A (Sigma), and 400 nM phenylmethylsulphonyl fluoride (PMSF) (Sigma) was added to cells once thawed on ice. Plates were subsequently scraped to collect lysates, followed by centrifugation at 4°C to separate cell debris. Resulting supernatants were collected, and protein was quantified by the Bradford method using Bio-Rad Protein Assay Dye Reagent. 20 µg of protein from lysates was boiled at 95°C for 15 minutes with 4x Laemmli buffer (Bio-Rad) supplemented with 10% β-mercaptoethanol (Sigma), and loaded into 4-15% TGX Precast gels (Bio-Rad). Gel electrophoresis was conducted using Bio-Rad Vertical Electrophoresis Cell systems at 180V filled with TGS running buffer until gels were suitably resolved. Bio-Rad Precision Plus Protein Dual Colour Standards protein ladder was added as a reference sample in each gel to calculate protein weight during western blotting.

After gel electrophoresis, western blot transfer was conducted using Bio-Rad Transblot Turbo Transfer Systems and Transfer Packs as per the manufacturer's instructions. Resulting nitrocellulose membranes were stained with Ponceau S stain to compare loading consistency between wells, followed by blocking with 5% non-fat milk in Tris-buffered saline with 0.1% Tween-20 (TBS/T) for 1 hour. Primary antibodies were then added to membranes and incubated overnight on a horizontal shaker at 4°C. All primary antibody dilutions used here were composed in a solution of TBS/T with 5% BSA (Table 5).

Table 5: List of the antibodies used in this study for western blot analysis.

Immunogen	Organism Source	Antibody Concentration Applied	Predicted Molecular Weight (kDa)	Manufacturer
SMN	Mouse	1:5000	40	BD (#610647)
B-actin	Rabbit	1:3000	45	Cell Signalling Technologies (13E5)
IMPA1	Rabbit	1:5000	30	Abcam (#ab184165)
ISYNA1	Rabbit	1:1000	61	Abcam (#ab118241)

1:5000 dilutions of species-specific secondary antibodies conjugated to horseradish peroxidase (HRP) in a 5% non-fat milk TBS/T solution were added to membranes for 1 hour. Clarity Western Enhanced Chemiluminescence (ECL) Substrate (Bio-Rad) was used to develop antibody bands on western blots, which was added to the membrane and incubated for 2 minutes. ECL was then removed, and the membrane was imaged using Bio-Rad Chemidoc systems. Images were imported into Bio-Rad ImageLab for analysis.

2.5 Seahorse

Seahorse Biosciences XFe96 Cell Culture Microplate were seeded with 20,000 cells per well in quadruplicate and incubated overnight in a humidified 37°C incubator with 5% (vol/vol) CO_2 overnight. A Seahorse XFe96 Sensor Cartridge was also hydrated by adding 200 µL of Seahorse XF Calibrant Solution to each well of the utility plate before lowering the cartridge into the wells. The cartridge-utility plate combination was then wrapped in cling film to reduce evaporation and left in a 37°C non-CO_2 incubator overnight.

DMEM without sodium bicarbonate (Sigma) was made freshly based on the specifications required by the assay, and buffered to pH 7.4 +/- 0.1. For the Glycolytic Stress Test, medium was supplemented with 1 mM sodium pyruvate and 2 mM L-glutamine, while the medium for the Mitochondrial Stress Test was supplemented similarly to the Glycolytic Stress Test with the addition of 10 mM glucose. Cell culture medium in Seahorse Microplates was removed and washed with Seahorse assay medium twice before adding assay media for a final volume of 175 µL in all wells. The microplates were then left to calibrate to assay conditions in a 37°C non-CO_2 incubator for an hour to remove any CO_2 that may interfere with ECAR measurements.

During microplate incubation in the non-CO_2 incubator, the Sensor Cartridge was removed from the non-CO_2 incubator and prepared with the compounds for injection. Each port was filled with 25uL of respective compound using an automated multichannel pipette. For the Glycolysis Stress Test, Port A was filled with 80 mM glucose for a final concentration after injection of 10 mM, Port B was filled with 18 µM oligomycin for a final concentration of 2 µM, and Port C was filled with 1 M 2-deoxy-D-glucose (2-DG) for a final concentration of 100 mM. For the Mitochondrial Stress Test, Port A was filled with 16 µM oligomycin for a final concentration of 2 µM, Port B was filled with 18 µM carbonyl cyanide 4-(trifluoromethoxy)phenylhydrazone (FCCP) for a final concentration of 2 µM, and Port C was filled with 5 µM of rotenone/antimycin A mixture for a final concentration of 0.5 µM. All drugs

were made up in medium respective to the Seahorse assay carried out. Once all ports were filled with their respective compounds, the loaded cartridge was inserted into the Seahorse XFe96 Bioanalyzer to calibrate. Following calibration, the cell microplate was ready to replace the calibrant utility plate in the Bioanalyzer after the hour incubation in the non-CO_2 incubator. Bioanalyzer protocol on Agilent WAVE software was as follows: 3 minute measure, 0 minute wait and 3 minute mix, where 5 measurements were taken before injection and 3 measurements were taken after each injection.

After completion of the assay, cell number was measured for normalisation using the CyQUANT Direct Cell Proliferation Assay (Thermo). Immediately after removal of the cell microplate, 150 µL of medium was removed from each well followed by addition of 100 µL of a 2x mixture of CyQUANT in PBS. The microplate was wrapped in aluminium foil and incubated at 37°C for 1 hour. After incubation, CyQUANT fluorescence was measured using a microplate reader set to measure excitation of 497nm and emission of 520nm.

2.6 ROS and Mitochondrial Membrane Potential Fluorescence

The fluorescent probes 5,6-chloromethyl-2',7'-dichlorodihydrofluorescein diacetate acetyl ester (CM-H_2DCFDA) (Invitrogen) and MitoSOX (Invitrogen), and the fluorescent dye tetramethylrhodamine ethyl ester (TMRE) (Invitrogen) were used to measure general ROS, mitochondrial superoxide and mitochondrial membrane potential respectively. For all experiments, 300,000 cells were seeded per well in a 6 well plate for each cell line in triplicate 48 hours before the experiment. Of these triplicate wells, one was to be unstained for background correction, another was stained with the probe/dye for basal measurements, and the last was stained with the probe/dye with the addition of treatment with a positive control agent.

For the DCFDA probe, the positive control well was washed with PBS and the medium was replaced with DMEM supplemented with 15% FBS and 5 mM *tert*-butyl hydroperoxide (TBHP) (Sigma), and incubated at 37°C for 2 hour. During this incubation, a vial of DCFDA probe was left to acclimatise to room temperature in dark conditions, followed by preparation of a 5 mM stock as per the manufacturer's instruction. A 5 µM working stock of DCFDA was then made in phenol red free and FBS free DMEM, with which 500 µL was used to replace the existing medium in the basal measurement wells and positive control, and incubated at 37°C for 30 minutes. After incubation with the DCFDA probe, the cells were washed with Hank's balanced salts solution (HBSS) and the cells from each well were trypsinised using phenol red free trypsin. Once detached, the cells were centrifuged, the trypsin aspirated, and the cell pellets re-suspended in 1 mL HBSS and transferred to flow cytometry tubes. Tubes were kept on ice until ready for flow cytometry using a BD LSR II Flow Cytometer using filter settings for detecting fluorescein (FITC) fluorescence.

For the MitoSOX probe, the positive control wells were treated with 5 µM rotenone for 15 minutes, followed by incubation with 5 µM MitoSOX probe. The cells were trypsinised and collected as per the procedure used for the DCFDA probe. Filter settings for detecting phycoerythrin (PE) fluorescence were used for flow cytometry.

For the TMRE dye, the positive control wells were treated with 100 µM FCCP for 15 minutes, followed by incubation with 100 nM TMRE for 20 minutes. The cells were trypsinised as per the previous procedures for flow cytometry and were re-suspended and collected with a PBS solution of 0.2% bovine serum albumin. Similarly, filter settings for detecting PE fluorescence were used for flow cytometry.

2.7 Metabolite Extractions for Liquid Chromatography/Mass Spectrometry

Extractions were performed on 70-80% confluent attached cells in 6 well plates in triplicate. A day prior to the extraction, an extraction solution was prepared comprised of 80% HPLC grade methanol and 20% HPLC grade water, which was left to cool at -80°C at least overnight. An hour before the extraction, medium was replaced with fresh medium and allowed to incubate at 37°C with 5% CO_2.

Metabolite extractions comprised of adding 1 mL cold 80% HPLC grade methanol prepared earlier to each well of attached cells after washing with cold PBS, and incubating for 15 minutes at -80°C. After incubation, each well was scraped, and the resulting homogenised cells were pipetted into tubes. Tubes were centrifuged at full speed for 15 minutes at 4°C. 700 µL of the supernatant was then pipetted into a separate labelled tube and set aside. A further 1 mL of cold 80% methanol was used to re-suspend the pellet from the first centrifugation, and centrifuged again for a further 15 minutes under the same conditions. 500 µL of the supernatant from this tube was removed and pooled with the previous 700 µL. This same process was repeated once more for a total of three pooled extractions per sample. All steps were performed on dry ice. The final tube containing the pooled supernatants of three metabolite extractions was then vacuum concentrated using a Savant SpeedVac Concentrator (Thermo) at room temperature until metabolite pellets are dried. Final pellets were stored at -80°C until samples were ready for sample submission for LC/MS. Dried metabolite pellets were re-suspended in 25 µL HPLC grade water for LC/MS. 1 µL of this metabolite suspension was analysed using Nexera X2 liquid chromatography system (Shimadzu) coupled to a QTRAP 6500 mass spectrometer (SCIEX) (Knott, et al., 2018).

2.8 Data Analysis

Seahorse data was preliminarily analysed using Agilent WAVE software, with further data analysis using Microsoft Excel and GraphPad Prism 7. Glycolysis stress test and mitochondrial stress test results were calculated as follows:

- Glycolysis = Max ECAR after glucose injection – Last ECAR before glucose injection
- Glycolytic Capacity = Max ECAR after oligomycin injection – Last ECAR before glucose injection
- Non-mitochondrial Respiration = Min OCR after R/A injection
- Basal Respiration = Last OCR before oligomycin injecton – Non-mitochondrial respiration
- Maximal Respiration = Max OCR after FCCP injection – Non-mitochondrial respiration
- ATP Production = Last OCR before oligomycin injection - Min OCR between oligomycin and FCCP injection
- Proton Leak = Min OCR between oligomycin and FCCP injection – Non-mitochondrial respiration

LC/MS peak intensities and chromatograms were analysed using SCIEX MultiQuant 1.1 software, which was exported to Microsoft Excel, GraphPad Prism 7 and R Studio for further analysis. Western blot data and densitometry was analysed using Microsoft Excel and Bio-Rad Image Lab. Flow cytometry data was analysed using Microsoft Excel, BD Biosciences FACSDiva, and Flowing Software. Statistical differences between groups were determined using an unpaired Student *t* test.

3. Results

3.1 SMA Fibroblast Model

3.1.1 Glycolytic Defects Are Evident In SMA Fibroblasts

Impaired glucose tolerance has been displayed as a feature in SMA patients and mice (Bowerman, et al., 2012), suggesting that glycolysis may be defective as a result of disturbances in glucose uptake from the blood. Furthermore, enrichment of the glycolytic enzyme PGK1 has been demonstrated in SMA resistant motor neuron populations in SMA zebrafish models; and overexpression of the aforementioned protein significantly rescues the defective motor neuron axonal phenotype observed in the same zebrafish model (Boyd, et al., 2017). Collectively, these findings suggest a role of glycolysis in SMA which we aimed to clarify.

To better understand a glycolytic alteration in SMA, we measured the extracellular acidification rates (ECAR) of fibroblasts derived from a family affected by SMA. Within this family, GM03813 fibroblasts derived from an SMA type I affected son, and GM03814 and GM03815 fibroblasts from disease-free carrier mother and father, respectively. ECAR, as measured using the Glycolytic Stress Test with the Agilent Seahorse XFe96 Bioanalyzer, represents the acidification of the medium from cells, which occurs primarily through the extrusion of lactate as a product of glycolysis.

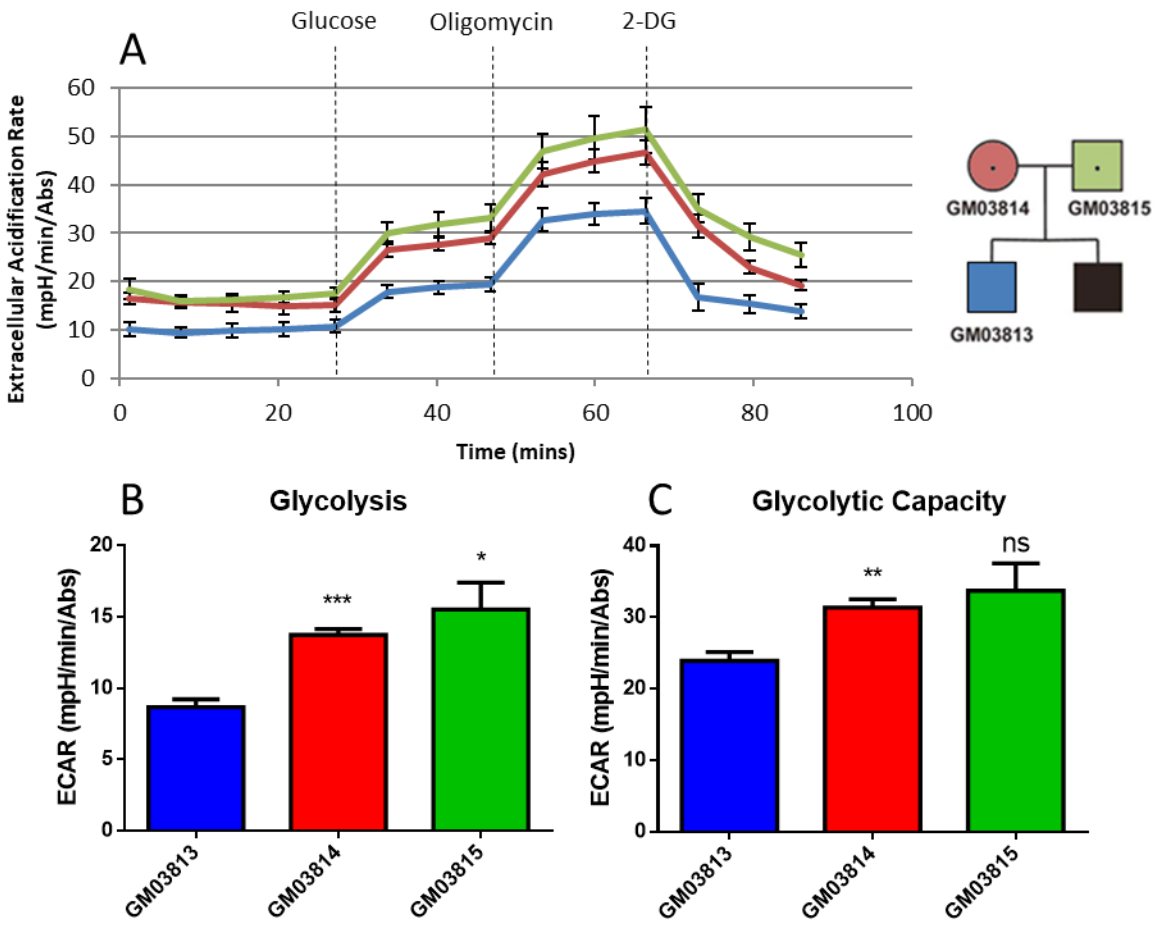

Figure 4: Fibroblasts derived from an SMA type I patient display defective glycolysis and glycolytic capacity. Agilent Biosciences Glycolysis Stress Test using Seahorse XFe96 Bioanalyzer measures extracellular acidification rate (ECAR) of cells under varying glycolytic stress conditions. (A) Line graph readout shows ECAR measurements of each population of cells taken every 6 minutes. The first 5 measurements are taken in the absence of glucose, followed by 3 measurements after an injection of glucose to stimulate glycolysis and subsequently increase ECAR, then 3 measurements after an injection of oligomycin to inhibit ATP synthesis thereby increasing the need for glycolysis to compensate for the lack of ATP, followed by a final 3 measurements after an injection of 2-deoxy-D-glucose (2-DG) which acts as a competitive inhibitor of hexokinase that inhibits glycolysis. (B) Glycolysis is represented by the difference between the max ECAR measurement after glucose injection and the last ECAR measurement before glucose injection, and (C) glycolytic capacity is represented by the difference between the max ECAR measurement after oligomycin injection and the last ECAR measurement before glucose injection. Asterisks above bars represent significant differences compared to GM03813 using unpaired two-tailed student t-test, where $p > 0.05$ = ns, $p < 0.05$ = *, $p < 0.01$ = **, $p < 0.001$ = ***, $p < 0.0001$ = ****.

The SMA type I fibroblasts GM03813 display lower ECAR levels before glucose administration, and even after injection of glucose, ECAR rises much less in this cell line compared to the SMA carrier fibroblasts GM03814 and GM03815 (Figure 4A). This difference in ECAR before and after the addition of glucose represents basal rates of glycolysis, where GM03813 utilises glucose much less than the two carrier fibroblasts (Figure 4B). Furthermore, inhibiting ATP synthase with oligomycin results in a smaller rise in ECAR from GM03813 than from GM03814 or GM03815 (Figure 4C). This indicates that under reduced mitochondrial ATP production, the fibroblasts sourced from an SMA type I patient are less able to use glycolysis to compensate for an energy deficit than the two SMA

carrier fibroblasts. Considering that mitochondrial ATP synthesis has been noted to be disrupted in SMA (Miller, Shi, Zelikovich, & Ma, 2016), it is interesting that glycolysis was less able to compensate for any mitochondrial shortcomings in ATP synthesis.

3.1.2 Mitochondrial Respiration Defects Are Evident In SMA Fibroblasts

Mitochondrial defects are an established feature of SMA, which have been reported in SMA patient muscle biopsies, SMA murine motor neurons and *in vitro* neuronal models (Berger, et al., 2003; Ascadi, et al., 2009; Ripolone, et al., 2015; Xu, Denton, Wang, Zhang, & Li, 2016; Miller, Shi, Zelikovich, & Ma, 2016). This raises an important question of whether ubiquitous SMN depletion results in mitochondrial dysfunction specifically in motor neurons and muscles through a tissue-specific interaction; or whether all tissues are all affected to a similar extent but the high energetic requirements of the affected tissues induces the specific vulnerability of motor neurons in SMA. To address this, we utilised the Mitochondrial Stress Test with the Seahorse Bioanalyzer to measure alterations in oxygen consumption rates (OCR) of the SMA type I fibroblasts GM03813, and the disease-free SMA carrier fibroblasts GM03814 and GM03815.

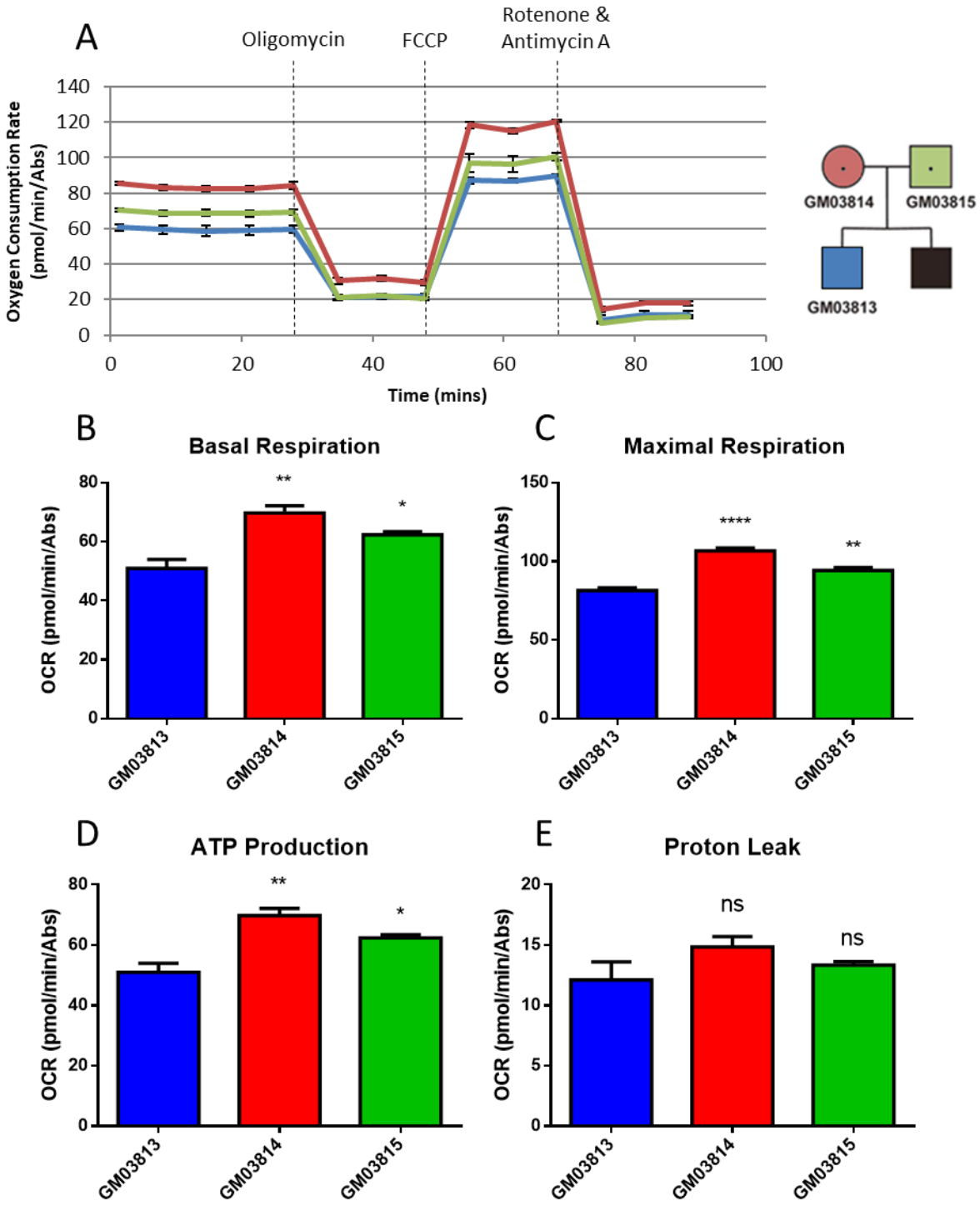

Figure 5: SMA type I patient fibroblasts GM03813 display defective basal and maximal respiration and reduced ATP production. Agilent Biosciences Mitochondrial Stress Test using Seahorse XFe96 Bioanalyzer is able to measure changes in oxygen consumption from cells in real-time – the primary site of oxygen consumption in the cell being the mitochondria. (A) Line graph readout showing the oxygen consumption of a population of fibroblasts under different mitochondrial stressors. Oxygen consumption rate (OCR) measurements are taken every 6 minutes, the first 5 of which are under basal conditions followed by 3 measurements after an injection of oligomycin to inhibit ATP synthase, then 3 measurements after an injection of FCCP to uncouple the electron transport chain thereby allowing all protons in the mitochondrial intermembrane space to be oxidised, followed by a

final 3 measurements after an injection of rotenone and antimycin A (R/A) to inhibit ETC complex I and III - respectively (B) Basal respiration is summarised by the last OCR measurement before oligomycin injection, (C) maximal respiration is summarized by the max OCR measurement after FCCP, (D) ATP production is summarised by the difference between the lowest OCR measurement after oligomycin and last OCR measurement before oligomycin injection, and (E) proton leak is summarized by the residual OCR after oligomycin injection. Accurate measurement of basal respiration, maximal respiration and proton leakage require subtraction of non-mitochondrial OCR, which is the lowest OCR measurement after R/A injection. Asterisks above bars represent significant differences compared to GM03813 using unpaired two-tailed student t-test, where $p > 0.05$ = ns, $p < 0.05$ = *, $p < 0.01$ = **, $p < 0.001$ = ***, $p < 0.0001$ = ****.

Under basal conditions, the SMA type I affected fibroblasts GM03813 display lower OCR compared to the two carrier fibroblasts (Figure 5A), indicating that without mitochondrial stressors, basal mitochondrial respiration was naturally lower in the SMA affected son compared to both control carrier parents (Figure 5B). Furthermore, introducing the mitochondrial uncoupling agent FCCP induced a much smaller increase in OCR in GM03813 compared to carrier controls GM03814 and GM03815, representing an impaired maximal respiration in GM03813 (Figure 5C). Oligomycin inhibits ATP synthase, halting proton flow into the mitochondrial matrix, and therefore a reduction in OCR is expected due to the activity of the aforementioned enzyme. Introducing oligomycin reduced basal respiration in GM03813 to a lesser extend than in the two carrier fibroblasts, suggesting that the SMA type I fibroblasts have a smaller ATP production ability through ATP synthase (Figure 5D).

Determining these parameters requires taking into account any sources of non-mitochondrial oxygen consumption. Inhibiting electron transport chain (ETC) complex I and III with rotenone and antimycin A, respectively, halts the flow of electrons to complex IV where oxygen is ultimately consumed to produce water (Li, Park, Deng, & Bai, 2006). In combination, these compounds eliminate mitochondrial oxygen consumption, therefore any OCR readings taken after injection of these drugs reflects non-mitochondrial OCR. This is important for determining proton leakage from mitochondria, where residual OCR after inhibiting complex I, III and ATP synthase represents the oxidation of protons leaking through the inner membrane into the matrix. Interestingly, while respiration and ATP synthesis was shown to be significantly diminished in the SMA type I fibroblasts, proton leakage was unaltered compared to the disease-free SMA carrier fibroblasts (Figure 5E). Proton leakage generally indicates inefficient mitochondrial coupling, resulting in reduced ATP production (Smith, Hartley, Cocheme, & Murphy, 2012). Defective mitochondrial bioenergetics without proton leakage, however, suggests that these respiration defects may not concern the maintenance of a proton gradient across the mitochondrial membrane. Considering that complex IV (Cytochrome *c* Oxidase) of the ETC has been reported to be deficient in SMA (Berger, et al., 2003), and that complex IV deficiency can induce a phenotype similar to SMA (Rubio-Gozalbo, et al., 1999; Salviati, et al., 2002), it is possible that defective ETC in SMA may be responsible for the mitochondrial dysfunction reported herein.

3.1.3 SMA Fibroblasts Display Reduced Reactive Oxygen Species and Impaired Mitochondrial Membrane Potential

The data presented here suggests that mitochondrial respiration defects are a feature of SMA in tissues other than motor neurons. A possible explanation for this mitochondrial dysfunction may be due to defective ETC, which is known to correlate with an increase in the production of destructive reactive oxygen species (ROS) (Murphy, 2009). Increased ROS has been reported by multiple sources

as a feature of mitochondrial dysfunction in murine and neuronal *in vitro* SMA models (Ascadi, et al., 2009; Miller, Shi, Zelikovich, & Ma, 2016; Xu, Denton, Wang, Zhang, & Li, 2016). However, there has been little consideration to whether elevated ROS is evident in other tissues due to ubiquitous SMN depletion.

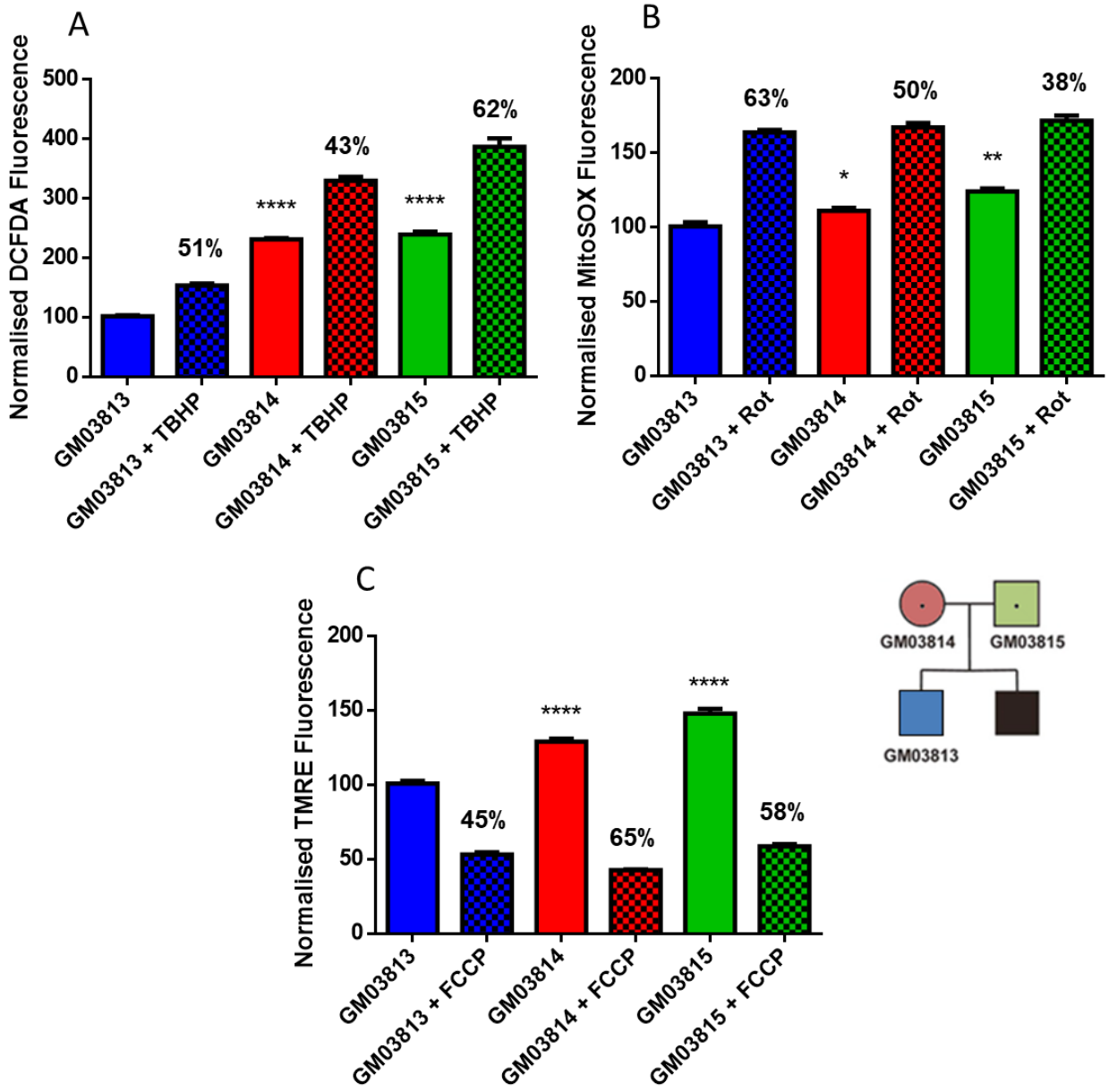

Figure 6: SMA type I patient fibroblasts GM03813 have reduced levels of ROS, mitochondrial superoxide, and mitochondrial membrane potential. (A) DCFDA fluorescence intensity values normalised to GM03813 fibroblasts. TBHP was used as a positive control to induce DCFDA fluorescence. (B) MitoSOX fluorescence intensity values normalised to GM03813 fibroblasts. Rotenone was used as a positive control to induce MitoSOX fluorescence. (C) TMRE fluorescence intensity values were normalised to GM03813 fibroblasts. FCCP was used as a positive control to reduce TMRE fluorescence. Percentage values above checked bars indicate the percent increase or decrease fluorescence when introduced to the positive control agent. Asterisks above bars represent significant differences compared to GM03813 using unpaired two-tailed student t-test, where $p > 0.05$ = ns, $p < 0.05$ = *, $p < 0.01$ = **, $p < 0.001$ = ***, $p < 0.0001$ = ****.

Using the General Oxidative Stress Indicator CM-H_2DCFDA, we are able to measure intracellular levels of ROS fluorometrically. This probe is able to diffuse into cells where intracellular esterases cleave the acetate groups, and CM-H_2DCFDA is now able to react with thiol containing compounds, that get subsequently oxidised (Eruslanov & Kusmartsev, 2010). The probe fluoresces after this oxidation, resulting in a probe that cannot exit the cell. Pre-treatment of cells with the cell permeable *tert*-butyl hydrogen peroxide (TBHP) elevates DCFDA fluorescence by increasing intracellular levels of hydrogen peroxide (H_2O_2), thereby acting as a positive control for high ROS (Roy & Sil, 2009). Interestingly, the SMA type I fibroblasts GM03813 exhibited a much lower fluorescence using this probe compared to the SMA carrier fibroblasts (Figure 6A) indicating that reduced ROS may be a feature of SMA type I fibroblasts.

The fluorescent mitochondrial superoxide indicator MitoSOX measures specifically superoxide ($O_2^{\bullet-}$) radicals. This subset of ROS is an important measurement of mitochondrial function because it is the product of oxygen reduction by electrons leaking from the ETC (Turrens, 2003). The positive charge of MitoSOX directs the molecule to the mitochondrial membrane where it fluoresces upon local oxidation by superoxide (Mukhopadhyay, et al., 2007). Pre-treating cells with the complex I inhibitor rotenone forces electrons out of the ETC and increases the production of superoxide (Li, Jen, Yu, & Hsiai, 2011), thus elevating MitoSOX fluorescence. Reflecting the reduced DCFDA fluorescence in Figure 6A, GM03813 also displays lower MitoSOX fluorescence compared to GM03814 and GM03815 control carriers (Figure 6B).

Finally, we used the fluorescent dye TMRE to measure mitochondrial membrane potential in the fibroblasts of the same SMA family. The positive charge of TMRE allows it to readily bind the mitochondrial membrane; however, the binding of the dye to the mitochondrial membranes relies on the membrane retaining its own negative charge. Weakening of the mitochondrial membrane proton gradient results in depolarisation of the mitochondrial membrane, which reduces the binding of TMRE to the membrane (Christensen, Jansen, Sanchez, & Waterhouse, 2013). Addition of the uncoupling agent FCCP allows protons to leak from the intermembrane space, therefore depolarising the outer membrane and acting as a positive control for TMRE (Joshi & Bakowska, 2011). Depolarised mitochondrial membrane is a pathological feature described in SMA motor neurons (Miller, Shi, Zelikovich, & Ma, 2016), however we aimed to expand on these findings to assess mitochondrial function in SMA fibroblasts. Indeed, TMRE fluorescence was reduced in the SMA type I fibroblasts compared to the two carrier controls, indicating that mitochondria in GM03813 have a lower membrane potential compared to GM03814 and GM03815 (Figure 6C).

3.2 SMN Knockdown Model

3.2.1 SMN Knockdown Causes a Glycolytic Defect in SMA Carrier Fibroblasts

Previously, we identified a glycolytic defect in SMA type I fibroblasts compared to fibroblasts derived from two disease-free SMA carriers. However, since the fibroblasts derived from the SMA family are sourced from three separate individuals, the differences described herein among GM03813, GM03814 and GM03815 may be caused by another genetic variability. In order to confirm that SMN depletion induces a glycolytic defect, we employed the Glycolytic Stress Test with stable lentiviral SMN knockdown in GM03814 carrier fibroblasts.

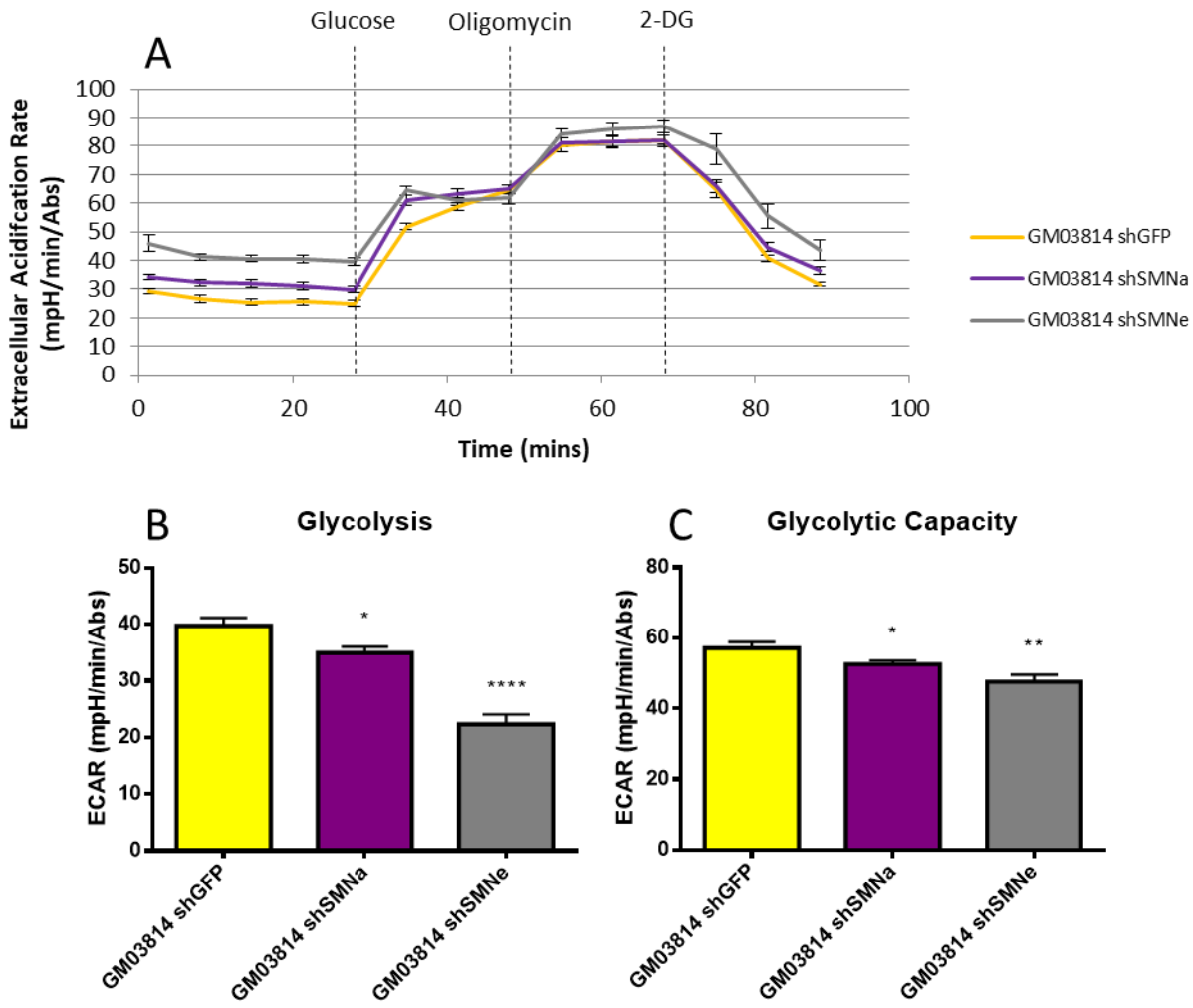

Figure 7: SMN knockdown in GM03814 SMA carrier fibroblasts induced similar glycolytic defects to those observed in SMA type I patient fibroblasts. ECAR levels were measured in GM03814 carrier fibroblasts treated with a stable lentiviral knockdown of SMN (shSMNa and shSMNe), or an shGFP control. (A) Line graph readout displays ECAR measurements taken every 6 minutes with compound injections as noted in Figure 4. (B) Glycolysis is represented by the difference between the max ECAR measurement after glucose injection and the last ECAR measurement before glucose injection, and (C) glycolytic capacity is represented by the difference between the max ECAR measurement after oligomycin injection and the last ECAR measurement before glucose injection. Efficiency of SMN knockdown can be observed in Figure 11B. Asterisks above bars represent significant differences compared to GM03814 shGFP using unpaired two-tailed student t-test, where $p > 0.05$ = ns, $p < 0.05$ = *, $p < 0.01$ = **, $p < 0.001$ = ***, $p < 0.0001$ = ****.

Knockdown of SMN led to a noticeable increase in ECAR before the addition of glucose, while glucose addition led to an increase in ECAR but to a similar level as shGFP (Figure 7A). Ultimately, this equates to a reduction in basal glycolysis, because ECAR was increased to a lesser extent in both knockdowns of SMN in response to glucose injection compared to the shGFP control (Figure 7B). Furthermore, ECAR increase was lower in both SMN knockdown fibroblasts in response to oligomycin compared to the shGFP control (Figure 7C), implying that SMN knockdown induces defects in both basal glycolysis and glycolytic capacity when mitochondrial ATP synthesis was inhibited. These results suggest that a glycolytic defect in SMA may be a direct response to SMN depletion.

3.2.2 SMN Knockdown Does Not Induce a Mitochondrial Defect in SMA Carrier Fibroblasts

Previously, we have identified mitochondrial defects in SMA fibroblasts (Figure 5). In order to clarify whether this feature was directly associated with SMN depletion, we employed the Mitochondrial Stress Test with stable lentiviral SMN knockdown in GM03814 carrier fibroblasts.

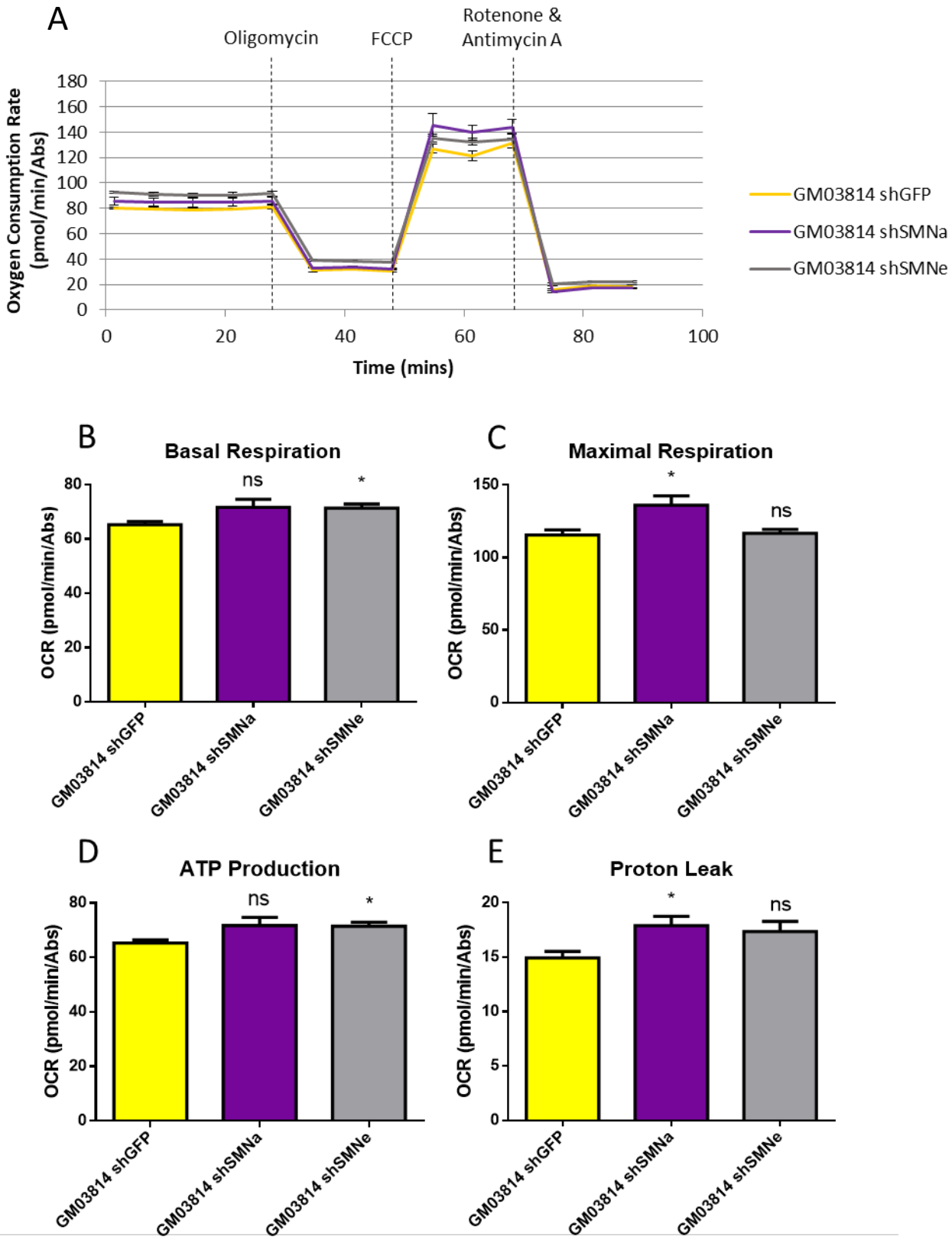

Figure 8: SMN knockdown in SMA GM03814 carrier fibroblasts does not induce a mitochondrial defect. OCR levels were measured in GM03814 fibroblasts treated with a stable lentiviral knockdown of SMN (shSMNa and shSMNe), or a shGFP control. (A) Line graph readout display OCR measurements taken every 6 minutes with compound injections as noted in Figure 5. (B) Basal respiration is summarised by the last OCR measurement before oligomycin injection, (C) maximal respiration is summarised by the max OCR measurement after FCCP, (D) ATP production is summarised by the difference between the lowest OCR measurement before oligomycin injection and the last OCR measurement before oligomycin injection, and (E) proton leak is summarised by the residual OCR after oligomycin injection. Basal respiration, maximal respiration and proton leakage take into account non-mitochondrial OCR. Efficiency of SMN knockdown can be observed in Figure 11B. Asterisks above bars represent significant differences compared to GM03814 shGFP using unpaired two-tailed student t-test, where $p > 0.05$ = ns, $p < 0.05$ = *, $p < 0.01$ = **, $p < 0.001$ = ***, $p < 0.0001$ = ****.

Interestingly, little difference in OCR was observed after SMN knockdown suggesting that SMN depletion may not directly induce mitochondrial dysfunction leading to an energy deficit (Figure 8A). SMN knockdown marginally elevated OCR, however OCR was not altered to the same degree as in GM03813 compared to GM03814 mother or GM03815 father (Figure 5). While the OCR difference between the fibroblasts in Figure 5 may be due to genetic variability between these family members, this is less likely among GM03813 and GM03814 due to the maternal mitochondrial relationship between these two individuals. Therefore, any mitochondrial differences between these two fibroblasts are more likely to be caused by SMA rather than a genetic variability.

3.2.3 SMN Knockdown Does Not Affect ROS to the Same Degree as in SMA Patients

Since SMN knockdown did not induce the same mitochondrial OCR defects observed in GM03813 fibroblasts, we aimed to elaborate on this by assessing whether ROS was altered under SMN knockdown in GM03814 fibroblasts. The fluorescent probes DCFDA, MitoSOX and the fluorescent dye TMRE were utilised as described in Figure 6, where general ROS, mitochondrial superoxide and mitochondrial membrane potential were measured in SMN knockdown GM03814 fibroblasts.

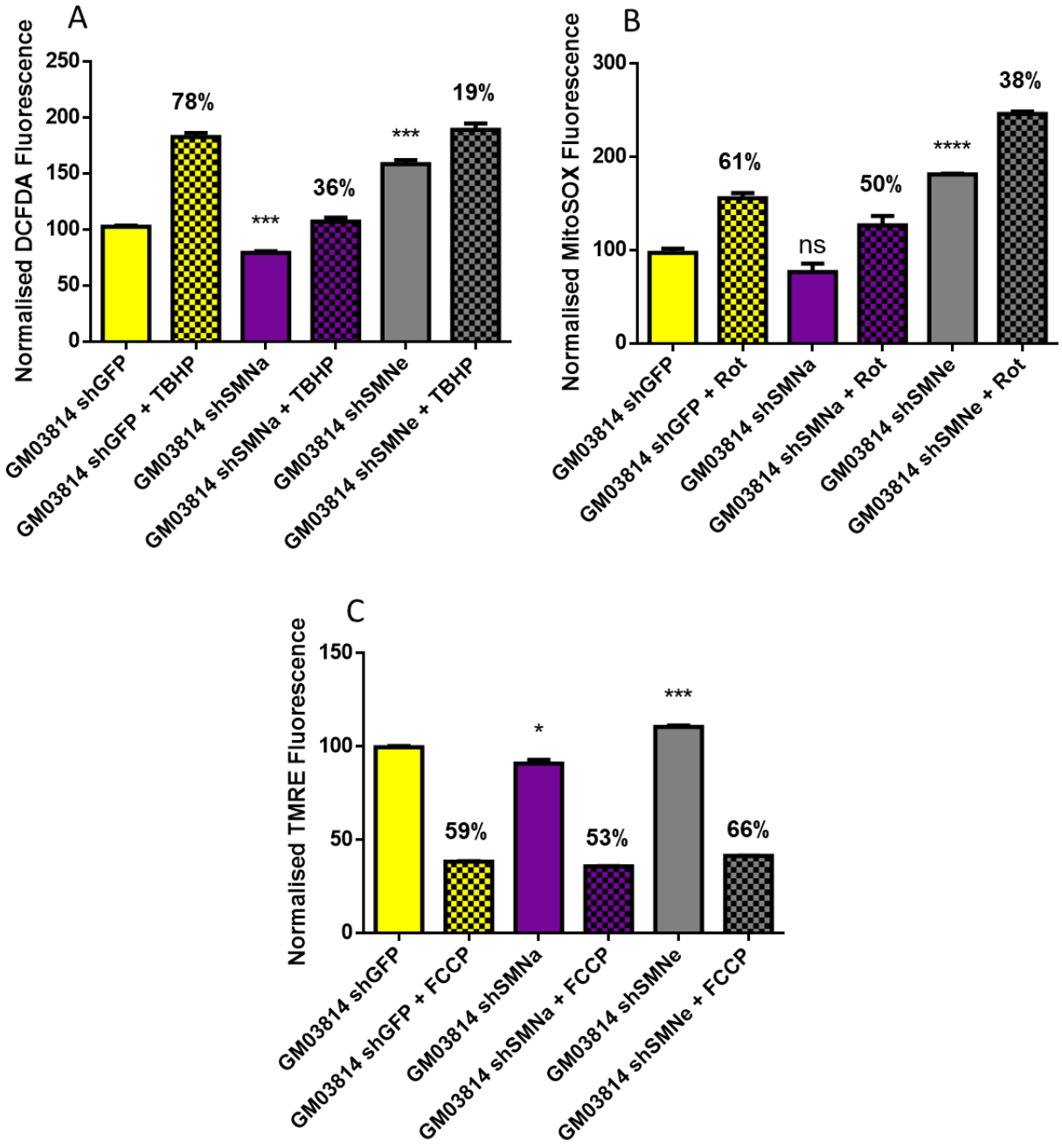

Figure 9: SMN knockdown in SMA carrier fibroblasts GM03814 does not alter ROS, mitochondrial superoxide or mitochondrial membrane potential as in SMA patient fibroblasts. (A) DCFDA fluorescence intensity values normalised to GM03814 shGFP fibroblasts. TBHP was used as a positive control to induce DCFDA fluorescence. (B) MitoSOX fluorescence intensity values normalised to GM03814 shGFP fibroblasts. Rotenone was used as a positive control to induce MitoSOX fluorescence. (C) TMRE fluorescence intensity values normalised to GM03814 shGFP fibroblasts. FCCP was used as a positive control to reduce TMRE fluorescence. Percentage values above checked bars indicate the percent increase or decrease fluorescence when introduced to the positive control agent. Efficiency of SMN knockdown can be observed in Figure 11B. Asterisks above bars represent significant differences compared to GM03813 using unpaired two-tailed student t-test, where $p > 0.05$ = ns, $p < 0.05$ = *, $p < 0.01$ = **, $p < 0.001$ = ***, $p < 0.0001$ = ****.

SMN knockdown in GM03814 using hairpin shSMNa induced a small decrease in ROS (Figure 9A) and mitochondrial membrane potential (Figure 9C), but did not alter mitochondrial superoxide (Figure 9B). However, the degree with which these parameters were reduced was negligible when compared to the reduction of ROS levels and mitochondrial membrane potential observed in GM03813 compared to the SMA carrier fibroblasts (Figure 6). Similarly, SMN knockdown induced marginal variation to mitochondrial OCR using the Mitochondrial Stress Test (Figure 8). SMN knockdown with shSMNe, however, induced a massive elevation in both DCFDA and MitoSOX fluorescence (Figure 9A and 9B), contrary to SMN knockdown with shSMNa. Considering that SMA fibroblasts display reduced ROS (Figure 6), the elevated ROS observed from shSMNe was likely to be a result of an off-target effect from this hairpin. Further examination into whether elevated ROS is a result of SMN depletion in fibroblasts is required to confirm if the phenotype seen from shSMNe herein was reliable.

3.3 LCMS Metabolomics

3.3.1 LCMS Analysis Reveals Common Metabolite Signatures among Type I SMA Patient and SMN Knockdown

Alterations in metabolic pathways can lead to disease states through imbalances in energetic systems, or through accumulation/deprivation of metabolites that would otherwise be strictly controlled in a healthy system (Xiao, Zhou, & Ressom, 2012). To assess the importance of the latter of these points, we utilised liquid chromatography/mass spectrometry (LCMS) to identify significantly upregulated or downregulated metabolites resulting from SMN depletion.

A

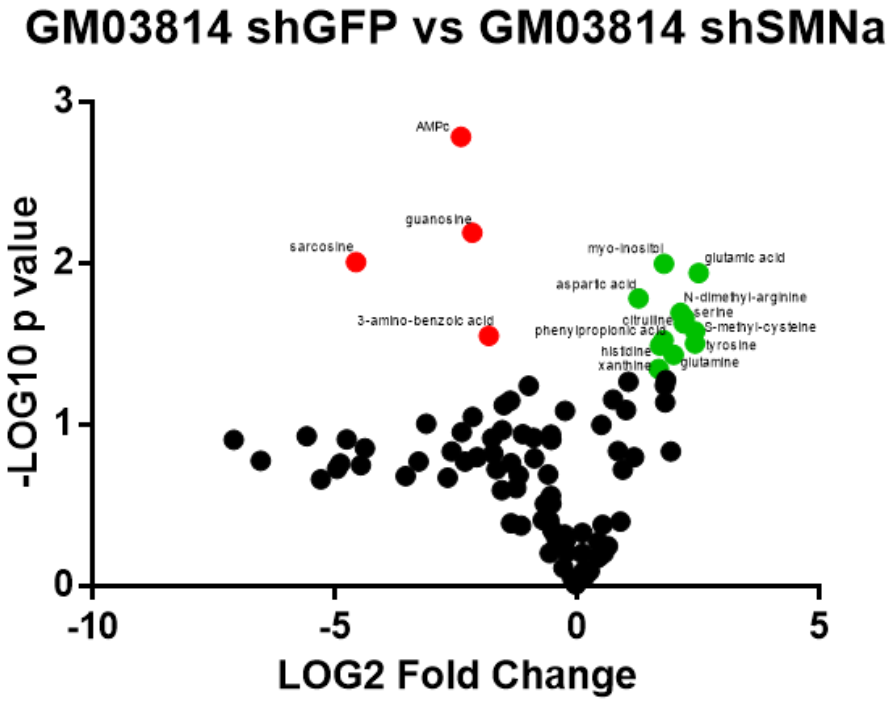

B

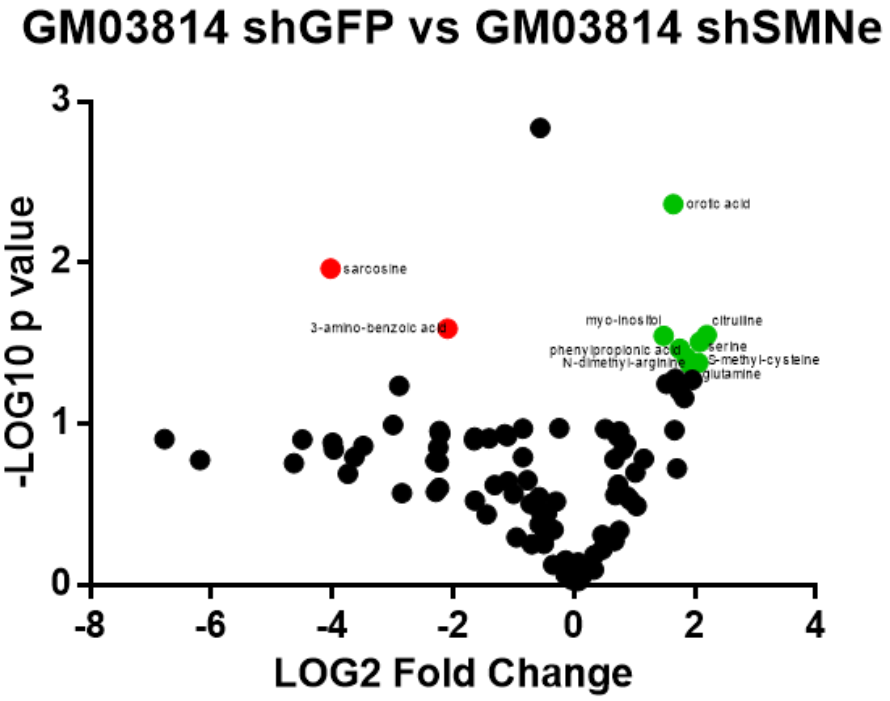

Figure 10: Metabolites are significantly altered after SMN knockdown in GM03814 fibroblasts. Volcano plots displaying metabolites with significantly altered metabolite peak intensity between (A) GM03814 shGFP and GM03814 shSMNa and (B) GM03814 shGFP and GM03814 shSMNe. Each point represents one metabolite measured, and coloured points indicate metabolites with a significant difference between shGFP and SMN knockdown (-Log10 p value > 1.3 = p value < 0.05) that also satisfied a cut-off point above 1 Log2 fold change or below -1 Log2 fold change . Red points depict metabolites that had lower peak intensity after SMN knockdown, and green points depict metabolites that had higher peak intensity in after SMN knockdown. Significant differences in metabolite peak intensity were determined using unpaired two-tailed student t-test.

In order to elucidate metabolite signatures in SMA, metabolites that were significantly altered between SMN knockdowns and shGFP control that also fulfilled the Log2 fold change cut-off point were first identified (Figure 10). After correcting for metabolites with weak chromatogram peaks compared to the LCMS reference samples, the remaining metabolites were then cross-referenced against metabolites altered between the SMA type I fibroblasts GM03813, and the SMA carrier fibroblasts GM03814 and GM03815. This stringent screening process ensures that metabolites that do not follow the same pattern within the family and knockdown fibroblasts are not erroneously followed up on. Sarcosine, for example, was significantly reduced in both SMN knockdown fibroblasts compared to shGFP and satisfied the cut-off point, yet was not significantly altered between GM03813 and either GM03814 or GM03815.

Of the metabolites analysed here, myoinositol (mI) was significantly upregulated in both SMN knockdowns compared to the shGFP control, as well as in GM03813 compared to both GM03814 and GM03815 SMA carriers (Figure 11A). Of particular note, while SMA carrier fibroblasts GM03815 present with low SMN protein levels (Figure 11B), mI levels in these fibroblasts are significantly lower than in the SMA type I fibroblasts GM03813, suggesting that elevated levels of mI are a feature of SMA. Furthermore, considering the relationship between mI and glucose metabolism (Dinicola, et al., 2017), we speculate that the accumulation of mI in SMA warrants further investigation.

3.3.2 *De Novo* Myoinositol Synthesis is Altered in SMA Fibroblasts

In order to assess the effect of mI upregulation in the SMA fibroblasts, we investigated alterations in relevant-associated ml pathways. mI is known to build up through two main pathways: influx through the mI-sodium co-transporter SLC5A3, or *de novo* biosynthesis from a glucose precursor (Di Daniel, Kew, & Maycox, 2009). Since we have described a glycolytic defect in both SMA patient fibroblasts and SMN knockdown in SMA carrier fibroblasts, we believed that the latter of these two pathways was most plausibly altered.

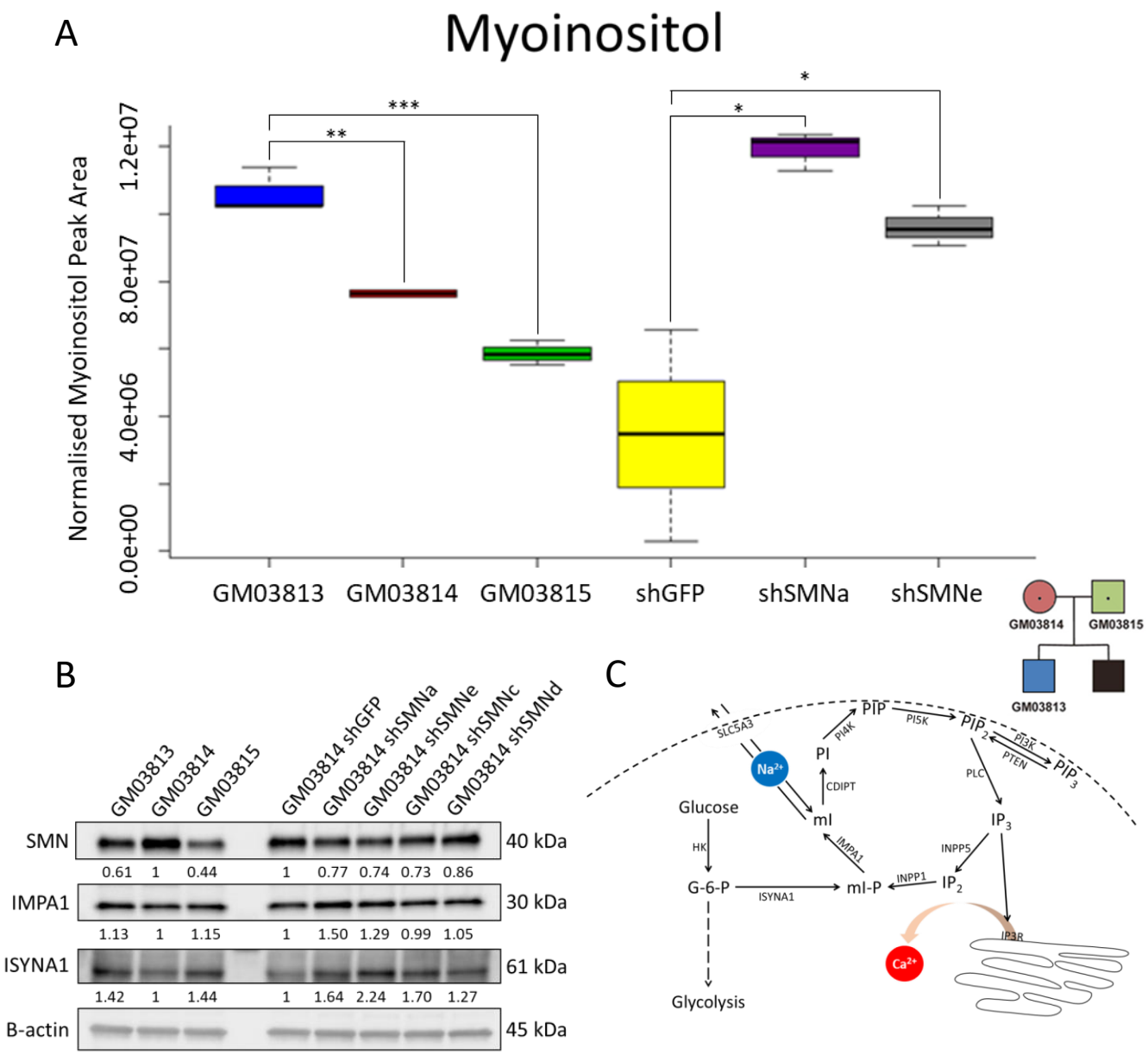

Figure 11: Myoinositol (mI) levels are elevated in both SMA type I patient fibroblasts GM03813 and SMN knockdown in GM03814 carrier fibroblasts due to elevated levels of *de novo* myoinositol synthesis pathway enzymes. (A) mI levels are significantly elevated in GM03813 fibroblasts compared to both SMA carrier fibroblasts, as well as both SMN knockdowns in GM03814 compared to the shGFP control. Asterisks above bars represent significant differences using unpaired two-tailed student t-test, where $p > 0.05$ = ns, $p < 0.05$ = *, $p < 0.01$ = **, $p < 0.001$ = ***, $p < 0.0001$ = ****. (B) *De novo* mI synthesis enzymes inositol-3-phosphate synthase (ISYNA1) and inositol monophosphatase (IMPA1) are both elevated upon SMN depletion in GM03813, GM03815 and a panel of SMN knockdowns in GM03814, as determined by western blot. (C) mI synthesis acts as an offshoot pathway of glycolysis, where once glucose has been phosphorylated by hexokinase (HK) into glucose-6-phosphate (G-6-P), the initial stage of inositol synthesis can begin. Inositol phosphate synthase (ISYNA1) creates the initial mI ring from G-6-P, which can then be dephosphorylated by inositol monophosphatase (IMPA1) to create mI. mI can also be exchanged with the extracellular matrix through the sodium cotransporter SLC5A3. Addition of glyceride groups to intracellular mI through CDP-diacylglycerol inositol phosphatidyltransferase (CDIPT) creates phosphatidylinositol (PI), which can be phosphorylated at any site free on the inositol ring. The best characterised use for

PI is through PI3K signalling, where phosphorylation of PI through PI4K and PI5K to create PIP_2 occurs at the intracellular side of the membrane. PIP_2 can be phosphorylated further by PI3K to create PIP_3, a metabolite important for growth and survival signalling through AKT. PTEN can reverse the action of PI3K however, to replenish PIP_2 , which can be recycled into the mI pool by cleavage of the glyceride groups through phospholipase C (PLC) to create inositol triphosphate (IP_3), followed by serial dephosphorylations through inositol polyphosphatases (INPP5 and INPP3). IP_3 is also an important intracellular signalling molecule, which is able to stimulate calcium release from the endoplasmic reticulum through activation of the inositol triphosphate receptor (IP3R) (Harwood, 2011).

mI is an alternative product from the glycolysis intermediate glucose-6-phosphate (G-6-P) (Bizzarri, Fuso, Dinicola, Cicina, & Bevilacqua, 2016). Two key enzymes are required for the synthesis of mI from G-6-P. First, inositol-3-phosphate synthase (ISYNA1) catalyses the cyclisation of G-6-P into mI-phosphate (mI-P), which is then dephosphorylated by inositol monophosphatase (IMPA1) to create mI (Rapaport, Primiani, Chen, Ahn, & Ryan, 2015). By western blot, levels of both ISYNA1 and IMPA1 were strikingly increased in both the SMA affected GM03813, and a range of SMN knockdowns (Figure 11B). Interestingly, levels of both of these enzymes were also elevated in GM03815, implying that the upregulation of *de novo* mI synthesis enzymes is dependent on SMN depletion, and that the subsequent regulation of this elevated mI synthesis may be responsible for sparing this individual from SMA. Considering the variety of function that mI can fulfil as a signalling molecule (Figure 11C), investigating the consequences of altered *de novo* mI synthesis in SMA might introduce a novel therapeutic opportunity.

4. Discussion

4.1 Main Findings

It has been well documented that depletion of the SMN protein causes SMA; however why loss of this ubiquitously expressed protein results in specifically motor neuron vulnerability remains a heavily debated issue (Monani, 2005). Given that SMN depletion has been shown to affect other tissues besides motor neurons (Malkki, 2016), investigating the metabolic features of other cell types from SMA patients could help with understanding the causative mechanisms of some of the clinical manifestations. In this study, we identify both a glycolytic and mitochondrial defect in an SMA type I patient, and that SMN knockdown in fibroblasts derived from a healthy SMA carrier is sufficient to induce a glycolytic defect. Furthermore, metabolomic profiling using LC/MS identified elevated mI as a feature in SMA type I fibroblasts and SMN knockdown carrier fibroblasts. This elevation in mI appears to be driven, at least in part, by increased levels of the *de novo* mI synthesis enzymes IMPA1 and ISYNA1, supporting a model whereby SMN depletion causes glucose to be redirected away from energy production from glycolysis towards mI synthesis. Collectively, these findings support the premise that metabolic processes responsible for energy production are commonly defective across affected and unaffected tissues from SMA patients opening new roads to novel therapeutic opportunities.

4.2 The Role of Glycolysis in SMA

While mitochondrial homeostasis has drawn the majority of the attention concerning metabolic defects in neurodegeneration, it is widely accepted that glucose acts as the primary fuel for the central nervous system (CNS) (Mergenthaler, Linauer, Dienel, & Meisel, 2013). Fatty acids as a metabolic fuel require extensive oxygen utilisation through β-oxidation potentially leading to hypoxia, and a larger yield of superoxide, which neurons are particularly susceptible to (Schönfeld & Reiser, 2013; Speijer, Manjeri, & Szklarczyk, 2014; Wang & Michaelis, 2010). Furthermore, amino acid metabolism in a neuronal setting generally increases toxic ammonia production and subsequently damages neurons (Honegger, et al., 2002). For these reasons, glucose remains the main energy substrate in the CNS (Camandola & Mattson, 2017). Since neurons have higher glucose dependencies than other cells, it stands to reason that glycolytic errors can be detrimental in a neuronal setting *in vivo*. Furthermore, since glycolysis provides an essential source of the Krebs cycle and the electron transport chain (ETC) intermediates for mitochondrial ATP production in neurons, glycolytic defects could impose detrimental effects on the cell's energy state both directly and indirectly through poorly supplied mitochondria. This fits with our hypothesis of an inefficient ETC that may not necessarily be damaged.

Here, we show that SMA affected fibroblasts are not only characterised by a glycolytic defect compared to carriers, but SMN knockdown alone is sufficient to induce this change. While drawing causation between SMN depletion and defective glucose utilisation in SMA would be premature, it is worth noting that a glycolytic defect was not identified in GM03815 (Figure 4) despite low SMN levels. Together with the hypothetical ability of GM03815 to prevent mI accumulation under SMN depletion (Figure 11A), it is plausible that the individual whom GM03815 fibroblasts were sampled from may remain asymptomatic by correcting the preference for mI synthesis over glycolysis

induced by SMN depletion – which was also apparent in the knockdown model (Figure 7). To further confirm this, assessing the activity of glycolytic enzymes in SMA affected fibroblasts would build credibility to the notion that glucose utilisation is different under SMN depletion.

Further evidence of the importance of glycolysis has been presented in a zebrafish model of SMA. Elevated expression of phosphoglycerate kinase 1 (PGK1) has been identified in motor neuron populations that were resistant to SMA progression, and PGK1 knockdown has been shown to phenocopy SMA (Boyd, et al., 2017). This fits with the current understanding of neuronal energetic demands, where neuronal synapses have highly dynamic energetic requirements during action potentials, and the instant bursts of ATP supplied by glycolysis are likely vital for signal transduction and subsequent neuronal homeostasis. To account for this high energy demand, glycolytic enzymes have been shown to localise across synapses in *C. elegans*, and loss of glucose uptake proteins such as GLUT4 can arrest synaptic vesicle uptake in a similar fashion to glucose withdrawal (Jang, et al., 2016; Ashrafi, Wu, Farrell, & Ryan, 2017). Collectively, these findings present an image of neurons fulfilling a large portion of energy requirements through glycolysis, and that impairment of this pathway neutralises their ability to achieve successful action potentials.

While a glycolytic defect may induce energetic deficiencies that impair neuronal function, it remains to be seen whether defects in glycolysis can be solely responsible for selective motor neuron vulnerability in SMA. Other sources that have also identified a glycolytic or oxidative phosphorylation defect in MNDs generally conclude that these impairments may result in a diminished energetic state, yet fail to explain why specifically motor neurons remain the primary neuronal tissue affected (Ascadi, et al., 2009). While it is possible that motor neurons have a much higher energy demand than any other neuronal cell types, this is yet to be shown. If this is the case, the wide range of SMA severities should present with degeneration of other tissue types due to varying grades of energetic impairments. While many highly energetic tissues have indeed been reported to be affected in SMA, other neuronal tissues in the CNS with high energy demands are spared. Therefore, additional consequences of SMN depletion may harmonise with energy deficiency to induce selective motor neuron degeneration observed in SMA.

4.2 The Role of Mitochondria in SMA

Mitochondrial dynamics are known to be altered in SMA, however the role of mitochondrial dysfunction in SMA pathophysiology is still unclear - whether it is defective bioenergetics, altered oxidative stress, faulty control and release of pro-apoptotic factors, or a combination of many mitochondrial functions (Ascadi, et al., 2009; Miller, Shi, Zelikovich, & Ma, 2016; Xu, Denton, Wang, Zhang, & Li, 2016).

Here we describe mitochondrial dysfunction in SMA fibroblasts presenting with reduced OCR, which is a strong indication for impaired respiration and concomitant decrease in energy production (Figure 5). Furthermore, these SMA fibroblasts have reduced general ROS, mitochondrial superoxide levels, and mitochondrial membrane potential (Figure 6). These findings suggest that mitochondria in these SMA type I fibroblasts are less efficient in energy production as a result of an impaired ability to maintain a healthy proton gradient. A likely explanation for this feature is that SMA causes alterations in ETC enzymes implying an increasing paucity of mitochondria. Interestingly, such

alterations in complex II and Cytochrome *c* have been reported in SMA affected cells, yet their mitochondrial number remains the same (Berger, et al., 2003). Furthermore, various reports of Cytochrome *c* Oxidase deficiency in infants resulting in a phenocopy of SMA reinforces a link between ETC alterations and SMA pathogenesis (Rubio-Gozalbo, et al., 1999; Salviati, et al., 2002).

Other groups have also noted mitochondrial dysfunction as a feature of SMA mouse model motor neurons, which was not recapitulated in midbrain neurons from the same animal (Miller, Shi, Zelikovich, & Ma, 2016). Collectively these data and our findings suggest that mitochondrial dysfunction is a feature of motor neurons and fibroblasts, but not other tissues such as midbrain neurons. It would therefore be prudent to investigate whether mitochondrial dynamics are altered in other tissues besides dermal fibroblasts. Considering the role of SMN in splicing machinery, it is possible that tissue-specific variants of mitochondrial proteins may be altered more severely in motor neurons and fibroblasts than in midbrain neurons giving rise to this variance. This has indeed been shown to be a feature in SMA mouse models, where changes in snRNAs varied between tissues, suggesting that splicing defects in SMA may also vary between tissues (Zhang, et al., 2008). Therefore, while mitochondrial proteins may be altered in spinal cord tissues, other tissues may be less affected. Identifying alternatively spliced mitochondrial proteins between SMA tissues is vital for assessing whether neuronal-specific mitochondrial dysfunction is an important pathogenic process in SMA.

Many reports of mitochondrial dysfunction in SMA assess the role of oxidative stress in pathogenesis (Berger, et al., 2003; Ascadi, et al., 2009; Miller, Shi, Zelikovich, & Ma, 2016; Patitucci & Ebert, 2016). Generation of ROS as a result of mitochondrial dysfunction can further exacerbate cell damage (Zorov, Juhaszova, & Sollott, 2014), and therefore may also be a driving factor for motor neuron degeneration. Increased free radical production has been described as a feature of mitochondrial dysfunction in SMN knockdown in murine motor neuron-like NSC-34 cells, and in SMA mouse motor neurons (Ascadi G. , et al., 2009; Miller, Shi, Zelikovich, & Ma, 2016). However, human iPSC-derived SMA astrocytes and motor neurons displayed no significant difference in mitochondrial respiration, and reduced ROS compared to a healthy control (Patitucci & Ebert, 2016). Furthermore, catalase expression in these astrocytes was found to be significantly elevated, suggesting an improved ability to metabolise ROS. Together with our findings, this suggests that elevated oxidative stress may only be a feature of SMA in murine models, whereas patient derived *in vitro* models of SMA presents with reduced oxidative stress. It would also be imperative to determine whether the reduced ROS observed in the SMA patient fibroblasts described herein is also due to enhanced expression of catalase.

4.3 Fibroblasts as a Model for SMA

Typically when modelling a disease, utilising the affected tissue *in vitro* will portray the pathological features. However, SMA presents a unique opportunity where aside the motor neurons which are primarily affected, patient-derived fibroblasts are commonly utilised to identify molecular mechanisms that may be altered under the disease state (Fuller, et al., 2016). The family fibroblast model described herein has been used by many other groups, and presents many vital controllable aspects for metabolic phenotyping. For example, the fibroblasts GM03813, GM03814 and GM03815 were all sampled from the same biopsy site (Table 4), which is ideal for characterising their

metabolism since different tissues vary in their bioenergetic requirements and metabolic profiles (Deidda, Piras, Bassareo, Seddalvi, & Mercuro, 2015). While this model can be advantageous for these experiments, obvious drawbacks must be accounted for, namely the genetic variability between the three individuals of the family model that may interfere with the results. For this reason, we introduced SMN knockdown experiments in GM03814 – the carrier mother – that had the highest endogenous SMN levels (Figure 11B).

The fibroblasts derived from the carrier father (GM03815) has been a riddle to many authors in the past, due to this cell line expressing very low levels of SMN, even lower than the SMA type I affected son, GM03813 (Figure 11B). It is known that the SMA affected son had a brother that also suffered from SMA, leading to some groups claiming that GM03815 was the brother rather than the father of GM03813 (Wan, et al., 2005). Through our own STR profiling (Supplementary Table 1), and digital PCR evidence from another group (Stabley, et al., 2017), we are confident that GM03815 is indeed the father of GM03813. This leaves some confusion as to why the father has lower levels of SMN than in the SMA type I son, yet according to Coriell Cell Repository, GM03815 was sourced from a clinically unaffected carrier. Various SMA genetic modifiers have been noted that may account for the asymptomatic state of this individual without modifying the endogenous SMN levels (Table 2) (Oprea, et al., 2008; Reissland, et al., 2017). However, identifying this modifier was beyond the scope of this study. It is, however, interesting to speculate why the carrier father was asymptomatic based on the metabolic features described in this study. For example, since mI was elevated only in the son and the SMN knockdowns (Figure 11A), perhaps the father is spared the disease by regulating mI biosynthesis despite SMN depletion. This raises an exciting hypothesis that elevated mI may provide a novel molecular link between SMN depletion and SMA that might be therapeutically amenable.

While SMA fibroblast models may provide an accessible model for SMA, eventual transfer into a neuronal model is inevitable for enhanced clinical accuracy. Therefore, while the findings described in this study may be features of SMA or SMN depletion in fibroblasts, they must be recapitulated in a neuronal setting before assessing whether there is potential for ameliorating any aspects of SMA *in vivo* through targeting mitochondria, glycolysis and/or mI biosynthesis.

4.4 Discrepancies between SMN Knockdowns

As mentioned previously, while the stable SMN knockdowns displayed consistent SMN depletion in GM03814 cells (Figure 11B); vast differences between the two knockdowns were observed in DCFDA and MitoSOX fluorescence. While SMN depletion in GM03814 shSMNa displayed a small drop in DCFDA and MitoSOX fluorescence, a rather large increase in the fluorescence of these two probes was observed in GM03814 shSMNe compared to the shGFP control (Figure 9A and 9B). Since marginal changes in mitochondrial function were observed in this model (Figure 8), it is suggested that these ROS alterations may be stemming from sources beside dysfunctional mitochondrial energetics.

While an off-target effect of these shRNAs must be considered, some insight into this inconsistency between the two shRNAs may lie within other data described herein. Using the metabolomics data acquired from LC/MS, we aimed to identify metabolites that may be causing elevated ROS in GM03814 shSMNe but not in GM03814 shSMNa. Orotic acid was one particular candidate, which

was found to be massively elevated in GM03814 shSMNe compared to both GM03814 shSMNa and the shGFP control (Supplementary Figure 1). Additionally, there was also no difference in orotic acid accumulation between the fibroblasts from the disease-affected family members. Dihydroorotate dehydrogenase (DHODH) is responsible for the synthesis of orotic acid from dihydroorotate, creating hydrogen peroxide as a by-product (Murphy, How mitochondria produce reactive oxygen species., 2009). It is possible that either this enzyme is overactive or the dihydroorotate precursor accumulates in GM03814 shSMNe creating this ROS discrepancy and elevated orotic acid. DHODH acts primarily within pyrimidine synthesis, and the only interaction between DHODH and mitochondrial function is its incorporation in the inner mitochondrial membrane and utilisation of complex III to metabolise the hydrogen peroxide created by orotic acid synthesis (Munier-Lehmann, Vidalain, Tangy, & Janin, 2013). While this process may explain the difference in ROS levels between the cell lines transfected with the two different shRNAs, further confirmation is necessary to confirm their specificity and/or that any changes are not due to any off target effects.

4.5 Myoinositol in Neurodegeneration

Here, we provide evidence that energy production from glycolysis may be impaired in SMA, therefore contributing to energetic deficiency. Glucose metabolism defects have been suggested in SMA as a result of impaired glucose intolerance in SMA patients, and a role of the glycolytic enzyme PGK1 has been described in populations of zebrafish motor neurons resisting degeneration (Bowerman, et al., 2012; Boyd, et al., 2017). However, there has been little consideration towards glycolysis as a producer of energy with regards to SMA. While redirecting glucose away from energy production may be an important part of SMA pathogenesis, the alternative production of mI from glucose may provide further insight to the molecular mechanisms underlying the disease. Here we also identify elevated *de novo* mI synthesis enzymes resulting at increased levels of mI in both SMA type I fibroblasts compared to carrier fibroblasts, and SMN knockdown fibroblasts compared to control.

Elevated mI has been identified in a plethora of neurodegenerative diseases including ALS (Filippa & Agosta, 2016), Alzheimer's disease (Voevodskaya, et al., 2016), Tay Sachs disease (Jamrozik, Królicki, Maczewska, & Kuźma-Kozakiewicz, 2013) and Huntington's disease (Sturrock, et al., 2015). Adding SMA to this list of neurodegenerative diseases with motor function involvement reinforces the rationale for assessing the importance of mI in MND pathogenesis.

The elevated levels of mI in neurodegenerative disorders were identified clinically using magnetic resonance spectroscopy (MRS) – a diagnostic tool that performs on a principle similar to magnetic resonance imaging (MRI). However, rather than measuring the abundance of water in the body, certain metabolite abundances can be measured non-invasively in a patient (Soares & Law, 2009). This technique is of particular importance in CNS conditions where biopsies impose a much larger risk than in other parts of the body. In the context of the CNS, mI is particularly concentrated in astrocytes, and therefore is commonly used as a marker for astrocytes and other glia using MRS (Merugumala, et al., 2014). Because of the propensity of astrocytes to accumulate mI, it is commonly used as a marker of astrogliosis in MRS – a feature commonly found late in the pathogenesis of SMA (Harris, Choi, & Brooks, 2015). mI is thought to primarily function as an osmolyte in the CNS by controlling sodium levels through the sodium/myoinositol cotransporter

SLC5A3 and, therefore, the osmotic stress imposed by sodium influx to regulate mI levels may contribute to SMA pathogenesis. Interestingly, a *C. elegans* ALS model has displayed hypersensitivity to osmotic stress, likely aggravating motor neuron degeneration, however the implications of osmotic stress in a motor neuron degenerative context has invited little consideration (Therrien, Rouleau, Dion, & Parker, 2013). While the role of mI as an osmolyte may have some implications towards motor neuron homeostasis, the role of inositol as a signalling molecule introduces many other functions.

Once introduced into the inositol cycle (Figure 11C), mI can be fed into PI3K signalling. Interestingly, PI3K involvement in SMA has been identified, where PTEN depletion has been shown to improve axon outgrowth, growth cone size and cell survival in SMN deficient murine motor neurons (Little, et al., 2015). Incorporating this evidence into the mI accumulation described herein implies that catalysing the conversion of PIP_3 to build up PIP_2 through PTEN may be detrimental to motor neuron health in SMA. It is thought that PTEN loss in this context is able to partially rescue these SMA motor neurons through activation of the pro-survival PI3K/AKT pathway. Furthermore, the U12 database (U12DB) shows that PTEN contains a U12 intron, which are thought to be preferentially mis-spliced under SMN depletion – drawing PTEN further into SMA pathogenesis. Therefore, it would be interesting to assess if the U12 intron retention events in SMA stabilise PTEN in order to over-perform its function, resulting in suppression of PI3K/AKT signalling that can be rescued following PTEN depletion *in vitro*. Additional investigation into the connection between PTEN, mI accumulation, and SMN depletion may be necessary to clarify whether targeting PTEN would be valuable for SMA therapeutics.

4.6 Elevated Myoinositol Has Implications for Calcium Regulation and Excitotoxicity

Calcium signalling has been shown to be overactive in SMA, where elevated intracellular calcium levels have been described in SMA affected murine muscle samples, and iPSC-derived astrocytes reprogrammed from GM03813 and GM03814 fibroblasts (Ruiz, Casañas, Torres-Benito, Cano, & Tabares, 2010; McGivern, et al., 2013). It was suggested that the most likely source of this calcium was aberrant calcium release from intracellular organelles rather than from extracellular sources, since mis-splicing and irregular clustering of calcium channel proteins has been described as a result of SMN depletion (Jablonka, Beck, Lechner, Mayer, & Sendtner, 2007; Sapaly, et al., 2018). Of these organelles, mitochondria can contribute to intracellular calcium release; hence the mitochondrial damage reported in SMA may lead to elevated calcium release. Notably, another source of intracellular calcium release is through the IP_3 receptor located on the endoplasmic reticulum. This mechanism would be worth exploring further considering IP_3 may be elevated when *de novo* mI synthesis is overactive. This concept is further reinforced since PTEN depletion is able to improve SMA symptoms (Little, et al., 2015), possibly by reducing the amount of IP_3 available to activate calcium release from the endoplasmic reticulum through the IP_3 receptor (Figure 11C). Since intracellular calcium levels have been shown to be elevated in SMA, and two possible methods of calcium release have been discussed herein, further investigation into the effects of calcium release in SMA may be necessary.

Elevated calcium levels have also been described in a range of neurodegenerative diseases with high levels of mI, further reinforcing a link between elevated mI and calcium homeostasis. For example,

ALS, Huntington's disease, Alzheimer's disease and Parkinson's disease have all been reported to present with elevated intracellular calcium levels, suggested to be stemming from irregular uptake or release of calcium from the mitochondria and/or endoplasmic reticulum (Patai, Nógrádi, Engelhardt, & Siklós, 2017). Calcium levels are normally strictly controlled at low intracellular concentrations, and are responsible for regulating a multitude of transcriptional, translational and metabolic processes (Brini, Calì, Ottolini, & Carafoli, 2014). However, aberrantly high concentrations of mI may push calcium levels above the homeostatic basal level (Berridge, 2015). This is of particular importance in motor neurons, which are distinctly vulnerable to calcium overload. Motor neurons have high expression of calcium-permeable AMPA receptors, and low expression of calcium buffering proteins responsible for controlling intracellular calcium levels, collectively increasing the risk of excitotoxicity (Vieira, et al., 2010; Leal & Gomes, 2015). Therefore, high levels of mI may give rise to specific motor neuron vulnerability by elevating calcium release through IP_3 receptors, which motor neurons are poorly equipped to handle.

Abnormal calcium regulation can also have implication for neuronal microenvironment cells surrounding motor neurons. Microglia, the local immune cells of the CNS, exhibit intense reactivity with calcium as a marker of tissue damage resulting in an inflammatory response (Brawek & Garaschuk, 2013; Deguise & Kothary, 2017). Elevated proinflammatory cytokines have also been shown to be a feature in SMA mouse models stemming from the microenvironment, namely astrocytes. In fact, restoration of SMN in the astrocytes of this SMA mouse model modestly improved survival (Rindt, et al., 2015). It is possible that the restoration of SMN allows these astrocytes to regulate mI levels, thereby reducing calcium release and subsequent microglia-mediated inflammatory reactions with neighbouring motor neurons.

Astrocytes accumulate near the end-stage of SMA in a state called astrogliosis, likely contributing to pathogenic processes including metabolic failure and inflammation (Sofroniew, 2009). These glia also exhibit a strong relationship with calcium, where astrocytes release gliotransmitters such as glutamate under rising intracellular calcium levels which can induce excitotoxicity in neighbouring motor neurons (Bazargani & Attwell, 2016). The main cause of this excitotoxicity is thought to be through activation of calcium channels, which are abundant on motor neurons, in order to induce calcium influx (Van Den Bosch, Van Damme, Bogaert, & Robberecht, 2006). However, increased calcium release from the endoplasmic reticulum due to pathogenically high levels of mI may hypothetically induce similar excitotoxicity – a feature which to our knowledge has yet to be explored in SMA.

These motor neuron-glia interactions have been explored in co-culture models where ALS-modelled astrocytes impose toxicity in healthy motor neurons both when cultured together, and through conditioned media (Lee, et al., 2016). A similar feature has been discussed using ALS-modelled oligodendrocytes, which were able to induce wild-type motor neuron death through hyperexcitability (Ferraiuolo, et al., 2016). This work stemmed from preliminary evidence showing that CSF sourced from ALS patients could induce a massive rise in intracellular calcium levels in cultured rat spinal neurons, specifically affecting motor neurons from these populations the most (Sen, Nalini, Joshi, & Joshi, 2005). While this evidence of possible calcium-induced glial reactivity in ALS offers insight into possible mechanisms leading to selective motor neuron degeneration in SMA, the relationship between motor neurons and the microenvironment requires further investigation.

One similar study of interest displayed reduced synapse number in wild-type motor neurons co-cultured with SMA astrocytes (Zhou, Feng, & Ko, 2016). However, it was deemed unlikely that this feature was due to calcium-dependant soluble factors such as gliotransmitters, since these synaptic defects were not seen in non-contact co-cultures between SMA astrocytes and wild-type motor neurons. Of note, contact signalling between astrocytes and motor neurons may be responsible and is facilitated through gap junctions which regulate the trafficking of signalling molecules such as IP_3 directly between cells (Belousov, Fontes, Freitas-Andrade, & Naus, 2017). Considering the predisposition of astrocytes to accumulate mI naturally, it is possible that SMN depletion further elevates mI, and subsequently IP_3 and calcium, imposing toxicity in neighbouring motor neurons through contact signalling (Decrock, et al., 2012; Merugumala, et al., 2014).

In order to assess the importance of mI accumulation in SMA pathology, it is imperative to clarify whether these calcium elevations in the disease state of SMA and ALS are dependent on mI. If this is the case, a possible therapeutic intervention may be useful by targeting the mI cycle and *de novo* mI synthesis to alleviate calcium accumulation, therefore preventing astrocyte-dependant excitotoxicity and microglial neuroinflammation.

4.7 Lithium and Valproic Acid as Regulators of Myoinositol Synthesis

While a handful of compounds targeting inositol synthesis have been developed, the application of these therapies is limited. The most well described use of this drug class is in the treatment of epilepsy and bipolar disorders (Grunze, 2010). Both lithium salts and valproic acid (VPA) have been shown to deplete intracellular mI levels, and MRS findings imply that elevated mI may be also a feature of bipolar disorder (Silverstone, McGrath, & Kim, 2005). However, whether elevated mI is a cause or a symptom of this disease is debated, as is the true target of these drugs.

Lithium is thought to have many mechanistic targets since the lithium ion is able to competitively inhibit enzymes that require magnesium cofactors (Ryves & Harwood, 2001). One target of particular interest, however, is the ability to inhibit IMPA1, likely resulting in mI depletion. This is the most widely accepted primary function of lithium in bipolar disorder, and the downstream reduction in IP_3 and subsequent decrease in intracellular calcium release is thought to account for lithium's neuroprotective effects (Alda, 2015).

The inositol depletion hypothesis fits the mechanism of action of VPA in bipolar disease as well; nevertheless this compound interacts with other enzymes that may induce the desired therapeutic effect through a separate mechanism. Concerning mI synthesis, VPA is thought to indirectly inhibit myoinositol phosphate synthase (MIPS) in yeast cells, which performs the same rate limiting step of converting glucose-6-phosphate (G-6-P) into myoinositol phosphate via ISYNA1 in humans (Yu & Greenberg, 2016). This is a likely explanation as to why inositol depletion is a feature of VPA treatment, however little work exploring how VPA interacts with ISYNA1 has been performed. It has been suggested that VPA inhibits ISYNA1 through glycogen synthase kinase 3 (GSK3), which is also thought to be another target of lithium (Yu, Daniel, Mehta, Maddipati, & Greenberg, 2017). While inositol depletion and GSK3 inhibition were originally thought to be contentious, they are actually complementary. ISYNA1 may have a GSK3 phosphorylation site, meaning that inhibition of GSK3 with VPA may reduce ISYNA1 activation, therefore reducing mI synthesis (Yu & Greenberg, 2016).

Furthermore, the canonical function of GSK3 is the control of the conversion of glycogen to glucose, and inhibiting GSK3 will reduce available G-6-P for mI synthesis. Another commonly accepted function of VPA is through the inhibition of histone deacetylaces (HDACs), where other HDAC inhibitors such as sodium butyrate have displayed similar promising effects in bipolar disease (Chuang, Leng, Marinova, Kim, & Chiu, 2009), further obscuring the therapeutic mechanisms of action of these drugs.

Interestingly, both lithium and VPA have been assessed for their therapeutic value in a number of neurodegenerative diseases since they seem to display neuroprotective effects (Leng, et al., 2008). Lithium has been suggested to reduce the risk of developing Alzheimer's disease (Nunes, Forlenza, & Gattaz, 2007), however whether this is due to alleviating mI accumulation has yet to be explored. The suggested neuroprotective effects of lithium has led to its application in ALS, where impressive positive results have been displayed at improving survival both in mouse models and human patients (Fornai, et al., 2008). Unfortunately, these results have yet to be reproduced, as despite being well tolerated, lithium has not significantly increased survival of ALS patients in more recent studies (Chiò & Mora, 2013; Petrov, Mansfield, Moussy, & Hermine, 2017). Again, while lithium has displayed varying value as a putative therapy for ALS, it has not been considered whether this therapeutic mechanism of action is through the depletion of mI.

The efficacy of VPA has been previously assessed in SMA. However, the ability of VPA to deplete mI has not been considered to be responsible for the therapeutic mechanism behind VPA (Yu & Greenberg, 2016). The HDAC inhibitor properties of VPA are thought to increase SMN protein expression by increasing the expression of the splicing factors responsible for *SMN2* transcription (Harahap, et al., 2012). While this has shown promise *in vitro*, VPA has proved ineffective at improving survival in clinical trials (Brichta, et al., 2003; Sumner, et al., 2003; Krosschell, et al., 2018). Interestingly, combination treatment of lithium and VPA displayed improved survival in an ALS clinical trial, further reinforcing the need to explore the mechanism behind the putative therapeutic benefits of these drugs in neurodegenerative diseases (Boll, et al., 2014).

Here we describe elevated mI as a feature of SMA, which may induce selective motor neuron vulnerability both through diverting glucose away from energy production, and by elevating intracellular calcium release through IP_3. It is therefore unusual that lithium and VPA have displayed limited success in ameliorating symptom in SMA and other similar diseases. If mI synthesis is to be the primary target of these drugs, dosage and delivery may need to be re-evaluated. Penetrance to motor neurons and astrocytes must also be considered, where perhaps intrathecal application may improve efficacy over the traditional formats used in bipolar disease and in past clinical trials. Since lithium and VPA have been suggested to reduce the activity of calcium signalling by reducing mI and IP_3 accumulation (Berridge, 2015), it seems prudent to reassess the utilisation of these drugs in neurodegenerative diseases, especially SMA.

4.8 Conclusions

Since mitochondrial dysfunction, elevated calcium and elevated mI have been described in SMA, it is tempting to speculate that redirecting glucose to create mI is detrimental to motor neurons on two fronts. Firstly, depleting ETC intermediates by reducing glycolytic function, thereby weakening ATP

production from both glycolysis and mitochondria; and secondly, elevating intracellular calcium levels through mitochondrial dysfunction and the IP_3 receptor on the endoplasmic reticulum leading to calcium overload. While motor neurons may be energetically demanding, this is unlikely to be the sole factor responsible for selective motor neuron vulnerability in SMA since other neuronal subtypes are spared. However, since motor neurons are particularly susceptible to calcium overload (Jaiswal, 2014), targeting calcium release from mitochondria and the endoplasmic reticulum as a result of mI accumulation may be effective. This feature combined with an energetic defect may produce the environment responsible for selective motor neuron degeneration. Therefore, reassessing the viability of mI depletive drugs in combination with mitochondrial protective therapies, such as Olesoxime (Bertini, et al., 2017), may introduce an effective and novel avenue of therapy for SMA.

5. References

Ahmad, S., Wang, Y., Shaik, G. M., Burghes, A. H., & Gangwani, L. (2012). The zinc finger protein ZPR1 is a potential modifier of spinal muscular atrophy. *Human Molecular Genetics, 21*(12), 2745-2758.

Alda, M. (2015). Lithium in the treatment of bipolar disorder: pharmacology and pharmacogenetics. *Molecular Psychiatry., 20*(6), 661.

Alías, L., Bernal, S., Fuentes-Prior, P., Barceló, M. J., Also, E., Martínez-Hernández, R., . . . Tizzano, E. (2009). Mutation update of spinal muscular atrophy in Spain: molecular characterization of 745 unrelated patients and identification of four novel mutations in the SMN1 gene. *Human genetics, 125*(1), 29-39.

Amano, M., Nakayama, M., & Kaibuchi, K. (2010). Rho-Kinase/ROCK: A Key Regulator of the Cytoskeleton and Cell Polarity. *Cytoskeleton, 67*(9), 545-554.

Ascadi, G., Lee, I., Li, X., Khaidakov, M., Pecinova, A., Parker, G. C., & Hüttemann, M. (2009). Mitochondrial dysfunction in a neural cell model of spinal muscular atrophy. *Journal of neuroscience research, 87*(12), 2748-2756.

Ashrafi, G., Wu, Z., Farrell, R. J., & Ryan, T. A. (2017). GLUT4 mobilization supports energetic demands of active synapses. *Neuron, 93*(3), 606-615.

Bazargani, N., & Attwell, D. (2016). Astrocyte calcium signaling: the third wave. *Nature neuroscience., 19*(2), 182.

Beattie, C. E., & Kolb, S. J. (2018). Spinal muscular atrophy: Selective motor neuron loss and global defect in the assembly of ribonucleoproteins. *Brain Research*.

Belousov, A. B., Fontes, J. D., Freitas-Andrade, M., & Naus, C. C. (2017). Gap junctions and hemichannels: communicating cell death in neurodevelopment and disease. *BMC Cell Biology, 18*(1), 4.

Berg, J. M., Tymoczko, J. L., & Stryer, L. (2002). *Biochemistry* (5th ed.). New York: WH Freeman.

Berger, A., Mayr, J. A., Meierhofer, D., Fötschl, U., Bittner, R., Budka, H., . . . Sperl, W. (2003). Severe depletion of mitochondrial DNA in spinal muscular atrophy. *Acta Neuropathologica, 105*(3), 245-251.

Berridge, M. J. (2015). The Inositol Trisphosphate/Calcium Signaling Pathway in Health and Disease. *Physiological Reviews., 96*(4), 1261-1296.

Bertini, E., Dessaud, E., Mercuri, E., Muntoni, F., Kirschner, J., Reid, C., . . . Fontoura, P. (2017). Safety and efficacy of olesoxime in patients with type 2 or non-ambulatory type 3 spinal muscular atrophy: a randomised, double-blind, placebo-controlled phase 2 trial. *The Lancet Neurology., 16*(7), 513-522.

Bevan, A. K., Huntchinson, K. R., Foust, K. D., Braun, L., McGovern, V. L., Schmelzer, L., . . . Kaspar, B. K. (2010). Early heart failure in the SMNΔ7 model of spinal muscular atrophy and correction by postnatal scAAV9-SMN delivery. *Human Molecular Genetics., 19*(20), 3895-3905.

Bizzarri, M., Fuso, A., Dinicola, D., Cicina, A., & Bevilacqua, A. (2016). Pharmacodynamics and pharmacokinetics of inositol (s) in health and disease. *Expert opinion on drug metabolism & toxicology, 12*(10), 1181-1196.

Boll, M. C., Bayliss, L., Vargas-Cañas, S., Burgos, J., Montes, S., Peñaloza-Solano, G., & Alcaraz-Zubeldia, M. (2014). Clinical and biological changes under treatment with lithium carbonate and valproic acid in sporadic amyotrophic lateral sclerosis. *Journal of the neurological sciences., 340*(1), 103-108.

Boulisfane, N., Choleza, M., Rage, F., Neel, H., Soret, J., & Bordonné, R. (2010). Impaired minor tri-snRNP assembly generates differential splicing defects of U12-type introns in lymphoblasts derived from a type I SMA patient. *Human Molecular Genetics, 20*(4), 641-648.

Bowerman, M., Anderson, C. L., Beauvais, A., Boyl, P. P., Witke, W., & Kothary, R. (2009). SMN, profilin IIa and plastin 3: a link between the deregulation of actin dynamics and SMA pathogenesis. *Molecular and Cellular Neuroscience, 42*(1), 66-74.

Bowerman, M., Michalski, J. P., Beauvais, A., Murray, L. M., DeRepentigny, Y., & Kothary, R. (2014). Defects in pancreatic development and glucose metabolism in SMN-depleted mice independent of canonical spinal muscular atrophy neuromuscular pathology. *Human Molecular Genetics, 23*(13), 3432-3444.

Bowerman, M., Murray, L. M., Boyer, J. G., Anderson, C. L., & Kothary, R. (2012). Fasudil improves survival and promotes skeletal muscle development in a mouse model of spinal muscular atrophy. *BMC medicine, 10*(1), 24.

Bowerman, M., Shafey, D., & Kothary, R. (2007). Smn depletion alters profilin II expression and leads to upregulation of the RhoA/ROCK pathway and defects in neuronal integrity. *Journal of Molecular Neuroscience, 32*(2), 120-131.

Bowerman, M., Swoboda, K. J., Michalski, J., Wang, G., Reeks, C., Beauvais, A., . . . Kothary, R. (2012). Glucose metabolism and pancreatic defects in spinal muscular atrophy. *Annals of Neurology., 72*(2), 256-268.

Boyd, P. J., Tu, W., Shorrock, H. K., Groen, E. J., Carter, R. N., Powis, R. A., . . . Gillingwater, T. H. (2017). Bioenergetic status modulates motor neuron vulnerability and pathogenesis in a zebrafish model of spinal muscular atrophy. *PLoS Genetics, 13*(4), e1006744.

Brawek, B., & Garaschuk, O. (2013). Microglial calcium signaling in the adult, aged and diseased brain. *Cell Calcium., 53*(3), 159-169.

Brichta, L., Hofmann, Y., Hahnen, E., Siebzehnrubl, F. A., Raschke, H., Blumcke, I., . . . Wirth, B. (2003). Valproic acid increases the SMN2 protein level: a well-known drug as a potential therapy for spinal muscular atrophy. *Human Molecular Genetics, 12*(19), 2481-2489.

Brini, M., Calì, T., Ottolini, D., & Carafoli, E. (2014). Neuronal calcium signaling: function and dysfunction. *Cellular and molecular life sciences., 71*(15), 2787-2814.

Burghes, A. H., & Beattie, C. E. (2009). Spinal Muscular Atrophy: Why do low levels of SMN make motor neurons sick? *Nature Reviews Neuroscience, 10*(8), 597.

Butchbach, M. E. (2016). Copy Number Variations in the Survival Motor Neuron Genes - Implications for Spinal Muscular Atrophy and Other Neurodegenerative Diseases. *Frontiers in Molecular Biosciences., 3*, 7.

Butchbach, M. E., Rose, F. F., Rhoades, S., Marston, J., T., M. J., Sinnott, R., & Lorson, C. L. (2010). Effect of diet on the survival and phenotype of a mouse model for spinal muscular atrophy. *Biochemical and biophysical research communications., 391*(1), 835-840.

Camandola, S., & Mattson, M. P. (2017). Brain metabolism in health, aging, and neurodegeneration. *The EMBO journal, 36*(11), 1474-1492.

Chang, J., Hsieh-Li, H., Jong, Y., Wang, N. M., Tsai, C., & Li, H. (2001). Treatment of spinal muscular atrophy by sodium butyrate. *Proceedings of the National Academy of Sciences, 98*(17), 9808-9813.

Chatwin, M., Bush, A., & Simonds, A. K. (2011). Outcome of goal-directed non-invasive ventilation and mechanical insufflation/exsufflation in spinal muscular atrophy type I. *Archives of Disease in Childhood , 96*(5), 426-432.

Chiò, A., & Mora, G. (2013). The final chapter of the ALS lithium saga. *Lancet Neurology., 12*, 324-325.

Christensen, M. E., Jansen, E. S., Sanchez, W., & Waterhouse, N. J. (2013). Flow cytometry based assays for the measurement of apoptosis-associated mitochondrial membrane depolarisation and cytochrome c release. *Methods, 61*(2), 138-145.

Chuang, D. M., Leng, Y., Marinova, Z., Kim, H. J., & Chiu, C. T. (2009). Multiple roles of HDAC inhibition in neurodegenerative conditions. *Trends in Neuroscience., 32*(11), 591-601.

Clelland, A. K., Kinnear, N. P., Oram, L., Burza, J., & Sleeman, J. E. (2009). The SMN Protein is a Key Regulator of Nuclear Architecture in Differentiating Neuroblastoma Cells. *Traffic, 10*(11), 1585-1598.

Coovert, D. D., Le, T. T., McAndrew, P. E., Strasswimmer, J., Crawford, T. O., Mendell, J. R., . . . Burghes, A. H. (1997). The survival motor neuron protein in spinal muscular atrophy. *Human Molecular Genetics, 6*(8), 1205-1214.

Corey, D. R. (2017). Nusinersen, an antisense oligonucleotide drug for spinal muscular atrophy. *Nature Neuroscience, 20*(4), 497.

Custer, S. K., Gilson, T. D., Li, H., Todd, A. G., Astroski, J. W., Liu, Y., & Androphy, E. J. (2016). Altered mRNA Splicing in SMN-Depleted Motor Neuron-Like Cells. *PloS One, 11*(10), e0163954.

D'Amico, A., Mercuri, E., Tiziano, F., & Bertini, E. (2011). Spinal Muscular Atrophy. *Orphanet Journal of Rare Diseases, 6*(1), 71.

David Arnold, W., Kassar, D., & Kissel, J. T. (2015). Spinal Muscular Atrophy: Diagnosis and Management in a New Therapeutic Era. *Muscle Nerve, 51*(2), 157-167.

Davis, R. H., Miller, E. A., Zhang, R. Z., & Swoboda, K. J. (2015). Responses to Fasting and Glucose Loading in a Cohort of Well Children with Spinal Muscular Atrophy Type II. *The Journal of pediatrics, 167*(6), 1362-1368.

Deguise, M., & Kothary, R. (2017). New insights into SMA pathogenesis: immune dysfunction and neuroinflammation. *Annals of Clinical and Translational Neurology., 4*(7), 522-530.

Deidda, M., Piras, C., Bassareo, P. P., Seddalvi, C. C., & Mercuro, G. (2015). Metabolomics, a promising approach to translational research in cardiology. *IJC Metabolic & Endocrine, 9*, 31-38.

Di Daniel, E., Kew, J. N., & Maycox, P. R. (2009). Investigation of the H+–myo-inositol transporter (HMIT) as a neuronal regulator of phosphoinositide signalling. *Biochemical Society Transactions, 37*(5), 1139-1143.

Dimitriadi, M., Derdowski, A., Kalloo, G., Maginnis, M. S., O'Hern, P., Bliska, B., . . . Hart, A. C. (2016). Decreased function of survival motor neuron protein impairs endocytic pathways. *Proceedings of the National Academy of Sciences., 113*(30), E4377-E4386.

Dimitriadi, M., Kye, M. J., Kalloo, G., Yersak, J. M., & Hart, A. C. (2013). The neuroprotective drug riluzole acts via small conductance Ca2+-activated K+ channels to ameliorate defects in spinal muscular atrophy models. *Journal of Neuroscience, 33*(15), 6557-6562.

Dinicola, S., Minini, M., Unfer, V., Verna, R., Cucina, A., & Bizzarri, M. (2017). Nutritional and Acquired Deficiencies in Inositol Bioavailability. Correlations with Metabolic Disorders. . *International journal of molecular sciences, 18*(10), 2187.

Doktor, T. K., Hua, Y., S., A. H., Brøner, S., Lio, Y. H., Wieckowska, A., . . . Andresen, B. S. (2017). RNA-sequencing of a mouse-model of spinal muscular atrophy reveals tissue-wide changes in splicing of U12-dependent introns. *Nucleic Acids Research, 45*(1), 395-416.

Dominguez, C. E., Cunningham, D., & Chandler, D. S. (2017). SMN regulation in SMA and in response to stress: new paradigms and therapeutic possibilities. *Human Genetics, 136*(9), 1173-1191.

Dupuis, L., Corcia, P., Fergani, A. G., Bonnefont-Rousselot, D., Bittar, R. S., Huaw, J., . . . Meininger, V. (2008). Dyslipidemia is a protective factor in amyotrophic lateral sclerosis. *Neurology, 70*(13), 1004-1009.

Dupuis, L., Oudart, H., René, F., Gonzalez de Aguilar, J., & Loeffler, J. (2004). Evidence for defective energy homeostasis in amyotrophic lateral sclerosis: Benefit of a high-energy diet in a transgenic mouse model. *Proceedings of the National Academy of Sciences of the United States of America., 101*(30), 11159-11164.

Eruslanov, E., & Kusmartsev, S. (2010). Identification of ROS using oxidized DCFDA and flow-cytometry. *In Advanced protocols in oxidative stress II*, 57-72.

Fallini, C., Bassell, G. J., & Rossoll, W. (2012). Spinal muscular atrophy: the role of SMN in axonal mRNA regulation. *Brain Research, 1462*, 81-92.

Farrar, M. A., Park, S. B., Vucic, S., Carey, K. A., Turner, B. J., Gillingwater, T. H., . . . Kiernan, M. C. (2017). Emerging therapies and challenges in spinal muscular atrophy. *Annals of Neurology, 81*(3), 355-368.

Ferraiuolo, L., Meyer, K., Sherwood, T. W., Vick, J., Likhite, S., Frakes, A., . . . Kaspar, B. K. (2016). Oligodendrocytes contribute to motor neuron death in ALS via SOD1-dependent mechanism. *Proceedings of the National Academy of Sciences., 113*(42), E6496-E6505.

Filippa, M., & Agosta, F. (2016). Does neuroinflammation sustain neurodegeneration in ALS? *Neurology, 87*(24), 2508-2509.

Fornai, F., Longone, P., Cafaro, L., Kastsiuchenka, O., Ferrucci, M., Manca, M. L., . . . Modugno, N. (2008). Lithium delays progression of amyotrophic lateral sclerosis. *Proceedings of the National Academy of Sciences., 105*(6), 2052-2057.

Fuller, H. R., Mandefro, B., Shirran, S. L., Gross, A. R., Kaus, A. S., Botting, C. H., . . . Sareen, D. (2016). Spinal Muscular Atrophy Patient iPSC-Derived Motor Neurons Have Reduced Expression of Proteins Important in Neuronal Development. *Frontiers in cellular neuroscience, 9*, 506.

Gabanella, F., Butchbach, M. E., Saieva, L., Carissimi, C., Burghes, A. H., & Pellizzoni, L. (2007). Ribonucleoprotein assembly defects correlate with spinal muscular atrophy severity and preferentially affect a subset of spliceosomal snRNPs. *PloS one, 2*(9), e921.

Gabanella, F., Pisani, C., Borreca, A., Farioli-Vecchioli, S., Ciotti, M. T., Ingegnere, T., & Monaco, L. (2016). SMN affects membrane remodelling and anchoring of the protein synthesis machinery. *Journal of Cell Science, 129*(4), 804-816.

Gabanella, F., Sarissimi, C., Usiello, A., & Pellizzoni, L. (2005). The activity of the spinal muscular atrophy protein is regulated during development and cellular differentiation. *Human Molecular Genetics, 14*(23), 3629-3642.

Garcera, A., Bahi, N., Peiyakaruppiah, A., Arumugam, S., & Soler, R. M. (2013). Survival motor neuron protein reduction deregulates autophagy in spinal cord motoneurons in vitro. *Cell death & disease, 4*(6), e686.

Gavrilov, D. K., Shi, X., Das, K., Gillam, T. C., & Wang, C. H. (1998). Differential SMN2 expression associated with SMA severity. *Nature Genetics, 20*(3), 230.

Grunze, H. C. (2010). Anticonvulsants in bipolar disorder. *Journal of mental health, 19*(2), 127-141.

Harahap, I. S., Saito, T., San, L. P., Sasaki, N., Nurputra, D., P., K., . . . Michio, H. (2012). Valproic acid increases SMN2 expression and modulates SF2/ASF and hnRNPA1 expression in SMA fibroblast cell lines. *Brain and Development, 34*(3), 213-222.

Harris, J. J., Jolivet, R., & Attwell, D. (2012). Synaptic Energy Use and Supply. *Neuron, 75*(5), 762-777.

Harris, J. L., Choi, I., & Brooks, W. M. (2015). Probing astrocyte metabolism in vivo: proton magnetic resonance spectroscopy in the injured and aging brain. *Frontiers in Aging Neuroscience., 7*, 202.

Harwood, A. J. (2011). Prolyl oligopeptidase, inositol phosphate signalling and lithium sensitivity. *CNS & Neurological Disorders-Drug Targets, 10*(3), 333-339.

Heimfarth, L., da Silva Ferreira, F., Pierozan, P., Loureiro, S. O., Mingori, M. R., Moreira, J. D., . . . Pessoa-Pureur, R. (2016). Calcium signaling mechanisms disrupt the cytoskeleton of primary astrocytes and neurons exposed to diphenylditelluride. *Biochimica et Biophysica Acta (BBA)-General Subjects, 1860*(11), 2510-2520.

Himilton, G., & Gillingwater, T. H. (2013). Spinal muscular atrophy: going beyond the motor neuron. *Trends in Molecular Medicine., 13*(1), 40-50.

Honegger, P., Braissant, O., Henry, H., Boulat, O., Backmann, C., Zurich, M., & Pardo, B. (2002). Alteration of amino acid metabolism in neuronal aggregate cultures exposed to hypoglycaemic conditions. *Journal of Neurochemistry, 81*(6), 1141-1151.

Hosseinibarkooie, S., Schneider, S., & Wirth, B. (2017). Advances in understanding the role of disease associated proteins in spinal muscular atrophy. *Expert Review of Proteomics, 14*(7), 581-592.

Ivings, L., Pennington, S. R., Jenkins, R., Weiss, J. L., & Buroyne, R. D. (2002). Identification of Ca2+-dependent binding partners for the neuronal calcium sensor protein neurocalcin delta: interaction with actin, clathrin and tubulin. *Biochemical Journal, 363*(3), 599.

Jablonka, S., Beck, M., Lechner, B. D., Mayer, C., & Sendtner, M. (2007). Defective Ca2+ channel clustering in axon terminals disturbs excitability in motoneurons in spinal muscular atrophy. *Journal of Cell Biology, 179*(1), 139-149.

Jaiswal, M. K. (2014). Selective vulnerability of motoneuron and perturbed mitochondrial calcium homeostasis in amyotrophic lateral sclerosis: implications for motoneurons specific calcium dysregulation. *Molecular and cellular therapies., 2*(1), 26.

Jamrozik, Z. Ł., Królicki, L., Maczewska, J., & Kuźma-Kozakiewicz, M. (2013). Late onset GM2 gangliosidosis mimicking spinal muscular atrophy. *Gene, 527*(2), 679-682.

Jang, S., Nelson, J. C., Bend, E. G., Rodríguez-laureano, L., Tueros, F. G., Cartagenova, L., . . . Cólon-Ramos, D. A. (2016). Glycolytic Enzymes Localize to Synapses under Energy Stress to Support Synaptic Function. *Neuron, 90*(2), 278-291.

Joshi, D. C., & Bakowska, J. C. (2011). Determination of mitochondrial membrane potential and reactive oxygen species in live rat cortical neurons. *Journal of visualized experiments: JoVE, 51*, 2704.

Kabashi, E., Bercier, V., Lissouba, A., Liao, M., Brustein, E., Rouleau, G. A., & Drapeau, P. (2011). FUS and TARDBP but Not SOD1 Interact in Genetic Models of Amyotrophic Lateral Sclerosis. *PLoS genetics, 7*(8), e1002214.

Kaczmarek, A., Schneider, S., Wirth, B., & Riessland, M. (2015). Investigational therapies for the treatment of spinal muscular atrophy. *Expert Opinion on Investigational Drugs., 24*(7), 867-881.

Kaifer, K. A., Villalón, E., Osman, E. Y., Glascock, J. J., Arnold, L. L., Corneloson, D. D., & Lorson, C. L. (2017). Plastin-3 extends survival and reduces severity in mouse models of spinal muscular atrophy. *JCI insight, 2*(5), e89970.

Kaksonen, M., & Roux, A. (2018). Mechanisms of clathrin-mediated endocytosis. *Nature Reviews Molecular Cell Biology, 19*(2), 71-135.

Kapitein, L. C., & Hoogenraad, C. C. (2015). Building the neuronal microtubule cytoskeleton. *Neuron, 87*(3), 492-506.

Kellogg, J., Bottman, L., Arra, E. J., Selkirk, S. M., & Kozlowski, F. (2017). Nutrition management methods effective in increasing weight, survival time and functional status in ALS patients: a systematic review. *Amyotrophic Lateral Sclerosis and Frontotemporal Degeneration., 19*(1), 1-5.

Knott, S., Wagenblast, E., Khan, S., Kim, S., Soto, M., Wagner, M., . . . Hannon, G. (2018). Asparagine bioavailability governs metastasis in a model of breast cancer. *Nature, 554*, 378-381.

Kolb, S. J., & Kissel, J. T. (2015). Spinal Muscular Atrophy. *Neurologics Clinics, 33*(4), 831-846.

Krosschell, K. J., Kissel, J. T., Townsend, E. L., Simeone, S. D., Zhang, R. Z., Reyna, S. P., . . . Swoboda, K. (2018). Clinical trial of L-Carnitine and valproic acid in spinal muscular atrophy type I. *Muscle & Nerve, 57*(2), 193-199.

Le Masson, G., Przedborski, S., & Abbott, L. F. (2014). A Computational Model of Motor Neuron Degeneration. *Neuron, 83*(4), 975-988.

Leal, S. S., & Gomes, C. M. (2015). Calcium dysregulation links ALS defective proteins and motor neuron selective vulnerability. *Frontiers in cellular neuroscience., 9*, 225.

Lee, J., Hyeon, S. J., Im, H., Ryu, H., Kim, Y., & Ryu, H. (2016). Astrocytes and microglia as non-cell autonomous players in the pathogenesis of ALS. *Experimental neurobiology., 25*(5), 233-240.

Lefebvre, S., Bürglen, L., Reboullet, S., Clermont, O., Burlet, P., Viollet, L., . . . Melki, J. (1995). Identification and characterization of a spinal muscular atrophy-determining gene. *Cell, 80*(1), 155-165.

Leng, Y., Liang, M. H., Ren, M., Marinova, Z., Leeds, P., & Chuang, D. M. (2008). Synergistic neuroprotective effects of lithium and valproic acid or other histone deacetylase inhibitors in neurons: roles of glycogen synthase kinase-3 inhibition. *28*(10), 2576-2588.

Li, R., Jen, N., Yu, F., & Hsiai, T. K. (2011). Assessing Mitochondrial Redox Status by Flow Cytometric Methods: Vascular Response to Fluid Shear Stress. *Current protocols in cytometry*, 9-37.

Li, Y., Park, J. S., Deng, J. H., & Bai, Y. (2006). Cytochrome c oxidase subunit IV is essential for assembly and respiratory function of the enzyme complex. *Journal of bioenergetics and biomembranes, 38*(5-6), 283-291.

Little, D., Valori, C. F., Mutsaers, C. A., Bennett, E. J., Wyles, M., Sharrack, B., . . . Ning, K. (2015). PTEN Depletion Decreases Disease Severity and Modestly Prolongs Survival in a Mouse Model of Spinal Muscular Atrophy. *Molecular Therapy, 23*(2), 270-277.

Lorson, C. L., Hahnen, E., Androphy, E. J., & Wirth, B. (1999). A single nucleotide in the SMN gene regulates splicing and is responsible for spinal muscular atrophy. *Proceedings of the National Academy of Sciences, 96*(11), 6307-6311.

Lotti, F., Imlack, W. L., Saieva, L., Beck, E. S., Hao, L. T., Li, D. K., . . . Pellizzoni, L. (2012). An SMN-Dependent U12 Splicing Event Essential for Motor Circuit Function. *Cell, 151*(2), 440-454.

Lunn, M. R., & Wang, C. H. (2008). Spinal muscular atrophy. *The Lancet, 37*(9630), 2120-2133.

Lyon, A. N., Pineda, R. H., Hao, L. T., Kudryashova, E., Kudryashov, D. S., & Beattie, C. E. (2014). Calcium binding is essential for plastin 3 function in Smn-deficient motoneurons. *Human molecular genetics, 23*(8), 1990-2004.

MacKenzie, A. E., & Gendron, N. H. (2001). Tudor reign. *Nature Structural & Molecular Biology, 8*, 13-15.

Malkki, H. (2016). Mitochondrial dysfunction could precipitate motor neuron loss in spinal muscular atrophy. *Nature Reviews Neurology, 12*(10), 560-562.

Martin, R., Gupta, K., Ninan, N. S., Perry, K., & Van Duyne, G. D. (2012). The Survival Motor Neuron protein forms soluble glycine zipper oligomers. *Structure, 20*(11), 1929-1939.

Matera, A. G., & Wang, Z. (2014). A day in the life of the spliceosome. *Nature reviews Molecular cell biology, 15*(2), 108.

Mattis, V. B., Rai, R., Wang, J., Chang, C. W., Coady, T., & Lorson, C. L. (2006). Novel aminoglycosides increase SMN levels in spinal muscular atrophy fibroblasts. *Human Genetics, 120*(4), 589-601.

McGivern, J. V., Patitucci, T. N., Nord, J. A., Barabas, M. E., Stucky, C., L., & Eberts, A. D. (2013). Spinal muscular atrophy astrocytes exhibit abnormal calcium regulation and reduced growth factor production. *Glia, 61*(9), 1418-1428.

Mendell, J. R., Al-Zaidy, S., Shell, R., Arnold, W. D., Rodino-Klapac, L., Prior, T. W., . . . Kaspar, B. K. (2017). AVXS-101 Phase 1 gene therapy clinical trial in SMA Type 1: Event free survival and achievement of developmental milestones. *European Journal of Paediatric Neurology., 21*, e13-e14.

Mercuri, E., Finkel, R. S., Muntoni, F., Wirth, B., Montes, J., Main, M., . . . Sejersen, T. (2018). Diagnosis and management of spinal muscular atrophy: part 1: recommendations for diagnosis, rehabilitation, orthopedic and nutritional care. *Neuromuscular Disorders, 28*(2), 103-115.

Mergenthaler, P., Linauer, U., Dienel, G. A., & Meisel, A. (2013). Sugar for the brain: the role of glucose in physiological and pathological brain function. *Trends in Neurosciences., 36*(10), 587-597.

Merugumala, S., Ramadan, S., Keenan, W., Liao, H., Wang, L. Y., & Lin, A. (2014). Magnetic Resonance Spectroscopy. *MRI in Psychiatry.*, 87-116.

Messina, S., Pane, M., De Rose, P., Vasta, I., Sorleti, D., Aloysuis, A., . . . Mercuri, E. (2008). Feeding problems and malnutrition in spinal muscular atrophy type II. *Neuromuscular Disorders, 18*(5), 389-393.

Miller, N., Shi, H., Zelikovich, A. S., & Ma, Y. C. (2016). Motor neuron mitochondrial dysfunction in spinal muscular atrophy. *Human Molecular Genetics., 25*(16), 3395-3406.

Mitchell, j. D., & Borasio, G. D. (2007). Amyotrophic lateral sclerosis. *The lancet, 369*(9578), 2031-2041.

Monani, U. R. (2005). Spinal muscular atrophy: a deficiency in a ubiquitous protein; a motor neuron-specific disease. *Neuron, 48*(6), 885-895.

Monani, U. R., Coovert, D. D., & Burghes, A. H. (2000). Animal models of spinal muscular atrophy. *Human Molecular Genetics, 9*(16), 2451-2457.

Monani, U. R., Lorsen, D., Parsons, W., Prior, T. W., Androphy, E. J., Burghes, A. H., & McPherson, J. D. (1999). A Single Nucleotide Difference That Alters Splicing Patterns Distinguishes the SMA Gene SMN1 From the Copy Gene SMN2. *Human Molecular Genetics, 8*(7), 1177-1183.

Monani, U. R., Sendtner, M., Coovert, D. D., Parson, D. W., Andreassi, C., Le, T. T., . . . Burghes, A. H. (2000). The human centromeric survival motor neuron gene (SMN2) rescues embryonic lethality in Smn–/– mice and results in a mouse with spinal muscular atrophy. *Human molecular genetics, 9*(3), 333-339.

Mukhopadhyay, P., Rajesh, M., Haskó, G., Hawkins, B. J., Madesh, M., & Pacher, P. (2007). Simultaneous detection of apoptosis and mitochondrial superoxide production in live cells by flow cytometry and confocal microscopy. *Nature Protocols, 2*(9), 2295.

Munier-Lehmann, H., Vidalain, P. O., Tangy, F., & Janin, Y. L. (2013). On dihydroorotate dehydrogenases and their inhibitors and uses. *Journal of medicinal chemistry., 56*(8), 3148-3167.

Murphy, M. P. (2009). How mitochondria produce reactive oxygen species. *Biochemical Journal, 417*(1), 1-13.

Nash, L. A., McFall, E. R., Perozzo, A. M., Turner, M., Poulin, K. L., De Repentigny, Y., . . . Parks, R. J. (2017). Survival Motor Neuron Protein is Released from Cells in Exosomes: A Potential Biomarker for Spinal Muscular Atrophy. *Scientific Reports, 7*(1), 13859.

Nunes, P. V., Forlenza, O. V., & Gattaz, W. F. (2007). Lithium and risk for Alzheimer's disease in elderly patients with bipolar disorder. *The British Journal of Psychiatry., 190*(4), 359-360.

Oprea, G. E., Kröber, S., McWhorter, M. L., Rossoll, W., Müller, S., Krawczak, M., . . . Wirth, B. (2008). Plastin 3 is a protective modifier of autosomal recessive spinal muscular atrophy. *Science, 320*(5875), 524-527.

Orrell, R. W. (2010). Motor neuron disease: systematic reviews of treatment for ALS and SMA. *British Medical Bulletin, 93*(1), 145-159.

Palamiuc, L., Schlagowski, A., Ngo, S. T., Vernay, A., Dirrig-Grosch, S., Henriques, A., . . . René, F. (2015). A metabolic switch toward lipid use in glycolytic muscle is an early pathologic event in a mouse model of amyotrophic lateral sclerosis. *EMBO Molecular Medicine., 7*(5), 526-546.

Patai, R., Nógrádi, B., Engelhardt, J. I., & Siklós, L. (2017). Calcium in the pathomechanism of amyotrophic lateral sclerosis–Taking center stage? *Biochemical and biophysical research communications, 483*(4), 1031-1039.

Patitucci, T. N., & Ebert, A. D. (2016). SMN deficiency does not induce oxidative stress in SMA iPSC-derived astrocytes or motor neurons. *25*(3), 514-523.

Pellizzoni, L., Charroux, b., Rappsilber, J., Mann, M., & Dreyfuss, G. (2001). A functional interaction between the survival motor neuron complex and RNA polymerase II. *The Journal of cell biology, 152*(1), 75-86.

Perera, N. D., & Turner, B. J. (2016). AMPK Signalling and Defective Energy Metabolism in Amyotrophic Lateral Sclerosis. *Neurochemical Research, 41*(3), 544-553.

Petrov, D., Mansfield, C., Moussy, A., & Hermine, O. (2017). ALS clinical trials review: 20 years of failure. Are we any closer to registering a new treatment? *Frontiers in Aging Neuroscience., 9*, 68.

Piras, A., Schiaffino, L., Boido, M., Valsecchi, V., Guglielmotto, M., De Amicis, E., . . . Vercelli, A. (2017). Inhibition of autophagy delays motoneuron degeneration and extends lifespan in a mouse model of spinal muscular atrophy. *Cell Death & Disease, 8*(12), 3223.

Potter, D. S., & Parker, R. (2016). Principles and properties of stress granules. *Trends in cell biology, 26*(9), 668-679.

Prior, T. W., Krainer, A. R., Hua, Y., Swoboda, K. J., Snyder, P. C., Bridgeman, S. J., . . . Kissel, J. T. (2009). A Positive Modifier of Spinal Muscular Atrophy in the SMN2 Gene. *The American Journal of Human Genetics, 85*(3), 408-413.

Rapaport, S. I., Primiani, C. T., Chen, C. T., Ahn, K., & Ryan, V. H. (2015). Coordinated expression of phosphoinositide metabolic genes during development and aging of human dorsolateral prefrontal cortex. *PloS one, 10*(7), e0132675.

Reissland, M., Kaczmarek, A., Schneider, S., Swoboda, K., Löhr, H., Bradler, C., . . . Wirth, B. (2017). Neurocalcin Delta Suppression Protects against Spinal Muscular Atrophy in Humans and across Species by Restoring Impaired Endocytosis. *The American Journal of Human Genetics, 100*(2), 297-315.

Renviosé, B., Khoobarry, K., Gendron, M. C., Cibert, C., Viollet, L., & Lefebvre, S. (2006). Distinct domains of the spinal muscular atrophy protein SMN are required for targeting to Cajal bodies in mammalian cells. *Journal of Cell Science, 119*(4), 680-692.

Rindt, H., Feng, Z., Mazzasette, C., Glascock, J. J., Valdivia, D., Pyles, N., . . . Lorson, C. (2015). Astrocytes influence the severity of spinal muscular atrophy. *Human Molecular Genetics., 24*(14), 4094-4102.

Ripolone, M., Ronchi, D., Violano, R., Vallejo, D., Fagiolari, G., Barca, E., . . . Moggio, M. (2015). Impaired Muscle Mitochondrial Biogenesis and Myogenesis in Spinal Muscular Atrophy. *JAMA neurology, 72*(6), 666-675.

Rossoll, W., & Bassell, G. J. (2009). Spinal Muscular Atrophy and a Model for Survival of Motor Neuron Protein Function in Axonal Ribonucleoprotein Complexes. *Cell Biology of the Axon, 48*, 87-107.

Rossoll, W., Jablonka, S., Andreassi, C., Kröning, A. K., Karle, K., Monani, U. R., & Sendtner, M. (2003). Smn, the spinal muscular atrophy–determining gene product, modulates axon growth and localization of β-actin mRNA in growth cones of motoneurons. *The Journal of cell biology, 163*(4), 801-812.

Roy, A., & Sil, P. C. (2009). Tertiary butyl hydroperoxide induced oxidative damage in mice erythrocytes: Protection by taurine. *Pathophysiology, 19*(2), 137-148.

Rubio-Gozalbo, M. E., Smeitink, J. A., Ruitenbeek, W., Ter Laak, H., Mullaart, R. A., Schuelke, M., . . . Gabreëls, F. J. (1999). Spinal muscular atrophy-like picture, cardiomyopathy, and cytochrome c oxidase deficiency. *Neurology, 52*(2), 383.

Rudnik-Schöneborn, S., Heller, R., Berg, C., Betzler, C., Grimm, T., Eggerman, T., . . . Zerres, K. (2008). Congenital heart disease is a feature of severe infantile spinal muscular atrophy. *Journal of Medical Genetics, 45*(10), 635-638.

Ruiz, R., Casañas, J. J., Torres-Benito, L., Cano, R., & Tabares, L. (2010). Altered intracellular Ca2+ homeostasis in nerve terminals of severe spinal muscular atrophy mice. *Journal of Neuroscience., 30*(3), 849-857.

Ryves, W. J., & Harwood, A. J. (2001). Lithium inhibits glycogen synthase kinase-3 by competition for magnesium. . *Biochemical and biophysical research communications, , 280*(3), 720-725.

Salviati, L., Sacconi, S., Rasalan, M. M., Kronn, D. F., Braun, A., Canoll, P., . . . DiMauro, S. (2002). Cytochrome c oxidase deficiency due to a novel SCO2 mutation mimics Werdnig-Hoffmann disease. *Archives of neurology, 59*(5), 862-865.

Santos, R. C., Bautista, S., Lucarelli, S., Bone, L. N., Dayam, R. M., Abousawan, J., . . . Antonescu, C. N. (2017). Selective regulation of clathrin-mediated epidermal growth factor receptor signaling and endocytosis by phospholipase C and calcium. *Molecular Biology of the Cell, 28*(21), 2802-2818.

Sapaly, D., Dos Santos, M., Delers, P., Biondi, O., Quérol, G., Houbedine, L., . . . Lefebvre, S. (2018). Small-molecule flunarizine increases SMN protein in nuclear Cajal bodies and motor function in a mouse model of spinal muscular atrophy. *Scientific Reports, 8*(1), 2075.

Schönfeld, P., & Reiser, G. (2013). Why does brain metabolism not favor burning of fatty acids to provide energy?-Reflections on disadvantages of the use of free fatty acids as fuel for brain. *Journal of Cerebral Blood Flow & Metabolism., 33*(10), 1498-1499.

Scoto, M., Finkel, R. S., Mercuri, E., & Muntoni, F. (2017). Therapeutic approaches for spinal muscular atrophy (SMA). *Gene Therapy, 24*(9), 514-519.

Sen, I., Nalini, A., Joshi, N. B., & Joshi, P. G. (2005). Cerebrospinal fluid from amyotrophic lateral sclerosis patients preferentially elevates intracellular calcium and toxicity in motor neurons via AMPA/kainate receptor. *Journal of the neurological sciences., 235*(1), 45-54.

Shlomi, T., Cabili, M. N., Herrgård, M. J., Palsson, B., & Ruppin, E. (2008). Network-based prediction of human tissue-specific metabolism. *Nature Biotechnology, 26*, 1003-1010.

Siegel, R., DeSantis, C., & Jemal, A. (2014). Colorectal cancer statistics. *CA: A Cancer Journal for Clinicians, 64*(2), 104-117.

Silverstone, P. H., McGrath, B. M., & Kim, H. (2005). Bipolar disorder and myo-inositol: a review of the magnetic resonance spectroscopy findings. *Bipolar Disorders, 7*(1), 1-10.

Singh, N. N., Howell, M. D., Androphy, E. J., & Singh, R. N. (2017). How the discovery of ISS-N1 led to the first medical therapy for spinal muscular atrophy. *Gene Therapy, 24*(9), 520.

Singh, R. K., & Cooper, T. A. (2012). Pre-mRNA splicing in disease and therapeutics. *Trends in Molecular Medicine, 18*(8), 472-482.

Singh, R. N., Howell, M. D., Ottesen, E. W., & Singh, N. N. (2017). Diverse role of survival motor neuron protein. *Biochimica et Biophysica Acta (BBA)-Gene Regulatory Mechanisms, 1860*(3), 299-315.

Smith, R. A., Hartley, R. C., Cocheme, H. M., & Murphy, M. P. (2012). Mitochondrial pharmacology. *Trends in pharmacological sciences, 33*(6), 341-352.

Soares, D. P., & Law, M. (2009). Magnetic resonance spectroscopy of the brain: review of metabolites and clinical applications. *Clinical radiology, 64*(1), 12-21.

Sofroniew, M. V. (2009). Molecular dissection of reactive astrogliosis and glial scar formation. *Trends in Neuroscience, 32*(12), 638-647.

Speijer, D., Manjeri, G. R., & Szklarczyk, R. (2014). How to deal with oxygen radicals stemming from mitochondrial fatty acid oxidation. *Philosophical Transactions B, 369*(1646), 20130446.

Stabley, D. L., Holbrook, J., Harris, A. W., Swoboda, K. J., Crawford, T. O., Sol-Church, K., & Butchbach, M. E. (2017). Establishing a reference dataset for the authentication of spinal muscular atrophy cell lines using STR profiling and digital PCR. *Neuromuscular Disorders., 27*(5), 439-446.

Stratigopoulos, G., Lanzano, P., Deng, L., Guo, J., Kaufmann, P., Darras, B., . . . Chung, W. K. (2010). Association of Plastin 3 Expression With Disease Severity in Spinal Muscular Atrophy Only in Postpubertal Females. *Archives of Neurology, 67*(10), 1252-1256.

Strong, M. J. (2010). The evidence for altered RNA metabolism in amyotrophic lateral sclerosis (ALS). *Journal of the neurological sciences, 288*(1), 1-12.

Sturrock, A., Laule, C., Wyper, K., Milner, R. A., Decolongon, J., Dar Santos, R., . . . Leavitt, B. R. (2015). A longitudinal study of magnetic resonance spectroscopy Huntington's disease biomarkers. *Movement Disorders., 30*(3), 393-401.

Sugarman, E. A., Nagan, N., Zhu, H., Akmaev, V. R., Zhou, Z., Rohlfs, E. N., . . . Allitto, B. A. (2012). Pan-ethnic carrier screening and prenatal diagnosis for spinal muscular atrophy: clinical laboratory analysis of >72 400 specimens. *European Journal of Human Genetics, 20*(1), 27.

Sumner, C. J., Huynh, T. N., Markowitz, J. A., Perhac, J. S., Hill, B., Coovert, D. D., . . . Fischbeck, K. H. (2003). Valproic acid increases SMN levels in spinal muscular atrophy patient cells. *Annals of Neurology, 54*(5), 647-654.

Taylor, J. P., Brown, R. H., & Cleveland, D. W. (2017). Decoding ALS: From Genes to Mechanism. *Nature, 539*(7628), 197-206.

Therrien, M., Rouleau, G. A., Dion, P. A., & Parker, J. A. (2013). Deletion of C9ORF72 results in motor neuron degeneration and stress sensitivity in C. elegans. *PloS one, 8*(12), e83450.

Tiryaki, E., & Horak, H. A. (2014). ALS and Other Motor Neuron Diseases. *CONTINUUM: Lifelong Learning in Neurology, 20*(5), 1158-1207.

Tisdale, S., & Pellizzoni, L. (2015). Disease Mechanisms and Therapeutic Approaches in Spinal Muscular Atrophy. *Journal of Neuroscience., 35*(23), 8691-8700.

Turrens, J. F. (2003). Mitochondrial formation of reactive oxygen species. *The Journal of Physiology, 552*(2), 335-344.

Turunen, J. J., Niemelä, E. H., Verma, B., & Frilander, M. J. (2013). The significant other: splicing by the minor spliceosome. *Wiley Interdisciplinary Reviews: RNA, 4*(1), 61-76.

Van Den Bosch, L., Van Damme, P., Bogaert, E., & Robberecht, W. (2006). The role of excitotoxicity in the pathogenesis of amyotrophic lateral sclerosis. *Biochimica et Biophysica Acta (BBA)-Molecular Basis of Disease., 1762*(11-12), 1068-1082.

Vander Heiden, M. G., Cantley, L. C., & Thompson, C. B. (2009). Understanding the Warburg effect: the metabolic requirements of cell proliferation. *Science, 324*(5930), 1029-1033.

Vieira, M., Fernandes, J., Burgeiro, A., Thomas, G. M., Huganir, R. L., Duarte, C. B., . . . Santos, A. E. (2010). Excitotoxicity through Ca2+-permeable AMPA receptors requires Ca2+-dependent JNK activation. *Neurobiology of disease, 40*(3), 645-655.

Vitte, J. N., Davoult, B., Roblot, N., Mayer, M., Joshi, V., Courageout, S., . . . Melki, J. (2004). Deletion of Murine Smn Exon 7 Directed to Liver Leads to Severe Defect of Liver Development Associated with Iron Overload. *American Journal of Pathology., 165*(5), 1731-1741.

Voevodskaya, O., Sungdren, P. C., Strandberg, O., Zetterberg, H., Minthon, L., Kaj, B., . . . Hansson, O. (2016). Myo-inositol changes precede amyloid pathology and relate to APOE genotype in Alzheimer disease. *Neurology., 86*(19), 1754-1761.

Wan, L., Battle, D. J., Yong, J., Gubitz, A. K., Kolb, S. J., Wang, J., & Dreyfuss, G. (2005). The survival of motor neurons protein determines the capacity for snRNP assembly: biochemical deficiency in spinal muscular atrophy. *Molecular and Cellular Biology., 25*(13), 5543-5551.

Wang, X., & Michaelis, E. K. (2010). Selective neuronal vulnerability to oxidative stress in the brain. *Frontiers in aging neuroscience, 2*, 12.

Weinberg, S. E., & Chandel, N. S. (2015). Targeting mitochondria metabolism for cancer therapy. *Nature Chemical Biology, 11*(1), 9-15.

Wirth, B., Brichta, L., Schrank, B., Lochmüller, H., Blick, S., Baasner, A., & Heller, R. (2006). Mildly affected patients with spinal muscular atrophy are partially protected by an increased SMN2 copy number. *Human Genetics, 119*(4), 422-428.

Wokke, J., Van Doorn, P., Hoogendijk, J., & De Visser, M. (2013). Spinal muscular atrophy type 3, Kugelberg–Welander disease. *Neuromuscular Disease: A Case-Based Approach*, 36-38.

Xiao, J. F., Zhou, B., & Ressom, H. W. (2012). Metabolite identification and quantitation in LC-MS/MS-based metabolomics. *TrAC Trends in Analytical Chemistry, 32*, 1-14.

Xu, C., Denton, K. R., Wang, Z., Zhang, X., & Li, X. (2016). Abnormal mitochondrial transport and morphology as early pathological changes in human models of spinal muscular atrophy. *Disease Models & Mechanisms, 9*(1), 39-49.

Yang, C., Chen, C., Chou, W., Lin, H., Jong, Y., Tsai, L., & Chuang, C. (2016). An Integrative Transcriptomic Analysis for Identifying Novel Target Genes Corresponding to Severity Spectrum in Spinal Muscular Atrophy. *PLoS One, 11*(6), e0157426.

Young, P. J., Day, P. M., Zhou, J., Androphy, E. J., Morris, G. E., & Lorson, C. L. (2002). A direct interaction between the survival motor neuron protein and p53 and its relationship to spinal muscular atrophy. *Journal of Biological Chemistry, 277*(4), 2852-2859.

Yu, W., & Greenberg, M. L. (2016). Inositol depletion, GSK3 inhibition and bipolar disorder. *Future Neurology., 11*(2), 135-148.

Yu, W., Daniel, J., Mehta, D., Maddipati, K. R., & Greenberg, M. L. (2017). MCK1 is a novel regulator of myo-inositol phosphate synthase (MIPS) that is required for inhibition of inositol synthesis by the mood stabilizer valproate. *PloS one, 12*(8), e0182534.

Zhang, H. L., Pan, F., Hong, D., Shenoy, S. M., Singer, R. H., & Bassell, G. J. (2003). Active transport of the survival motor neuron protein and the role of exon-7 in cytoplasmic localization. *Journal of Neuroscience, 23*(16), 6627-6637.

Zhang, H., Xing, L., Rossoll, W., Wichterle, H., Singer, R. H., & Bassell, G. J. (2006). Multiprotein complexes of the survival of motor neuron protein SMN with Gemins traffic to neuronal processes and growth cones of motor neurons. *Journal of Neuroscience, 16*(33), 8622-8632.

Zhang, Z., Lotti, F., Dittmar, K., Younis, I., Wan, L., Kasim, M., & Dreyfuss, G. (2008). SMN deficiency causes tissue-specific perturbations in the repertoire of snRNAs and widespread defects in splicing. *Cell, 133*(4), 585-600.

Zhang, Z., Pinto, A. M., Wan, L., Wang, W., Berg, M. G., Oliva, I., . . . Dreyfuss, G. (2013). Dysregulation of synaptogenesis genes antecedes motor neuron pathology in spinal muscular atrophy. *Proceedings of the National Academy of Sciences, 110*(48), 19348-19353.

Zhou, C., Feng, Z., & Ko, C. (2016). Defects in Motoneuron–Astrocyte Interactions in Spinal Muscular Atrophy. *Journal of Neuroscience., 26*(8), 2543-2553.

Zorov, D. B., Juhaszova, M., & Sollott, S. J. (2014). Mitochondrial Reactive Oxygen Species (ROS) and ROS-Induced ROS Release. *Physiological Reviews, 94*(3), 909-950.

Zou, J., Barahmand-pour, F., Blackburn, M. L., Matsui, Y., Chansky, H. A., & Yang, L. (2004). Survival motor neuron (SMN) protein interacts with transcription corepressor mSin3A. *Journal of Biological Chemistry, 279*(15), 14922-14928.

Zou, T., Yang, X., Pan, D., Huang, J., Sahin, M., & Zhou, J. (2011). SMN deficiency reduces cellular ability to form stress granules, sensitizing cells to stress. *Cellular and molecular neurobiology, 31*(4), 541-550.

Zufiria, M., Gil-Bea, F. J., Fernández-Torrón, R., Poza, J. J., Muñoz-Blanco, J. L., Rojas-García, R., . . . López de Munain, A. (2016). ALS: A bucket of genes, environment, metabolism and unknown ingredients. *Progress in Neurobiology, 142*, 104-129.

6. Supplementary Figures

Supplementary Table 12: GM03814 and GM03815 are respectively maternally and paternally related to GM03813. STR profiling results courtesy of Eurofins Forensics Services. It was concluded that the probability that the donor of the cell line GM03815 is the biological father of the donor of the cell line GM03813 is > 99.9999 %, and that the probability that the donor of the cell line GM03814 is the biological mother of the donor of the cell line GM03813 is 99.9998 %.

DNA-System	DNA-criteria GM03813 CL170822_001	DNA-criteria GM03814 CL170822_002	DNA-criteria GM03815 CL170822_003
AM	X, Y	X, X	X, Y
D3S1358	15, 17	15, 18	17, 18
D1S1656	11, 16	11, 17.3	13, 16
D6S1043	12, 15	12, 14	11, 15
D13S317	9, 11	11, 12	9, 11
Penta E	12, 16	16, 18	12, 18
D16S539	11, 12	11, 11	11, 12
D18S51	15, 17	15, 19	12, 17
D2S1338	22, 24	17, 24	18, 22
CSF1PO	9, 10	9, 10	10, 12
Penta D	12, 12	9, 12	12, 12
TH01	6, 7	6, 7	6, 9.3
vWA	16, 17	14, 16	14, 17
D21S11	29, 30	29, 29	30, 30
D7S820	9, 10	10, 10	9, 10
D5S818	11, 13	12, 13	11, 12
TPOX	8, 8	8, 11	8, 12
D8S1179	10, 12	12, 13	10, 15
D12S391	15, 18	18, 20	15, 21
D19S433	14, 14	14, 14	14, 15
FGA	20, 20	19, 20	20, 20

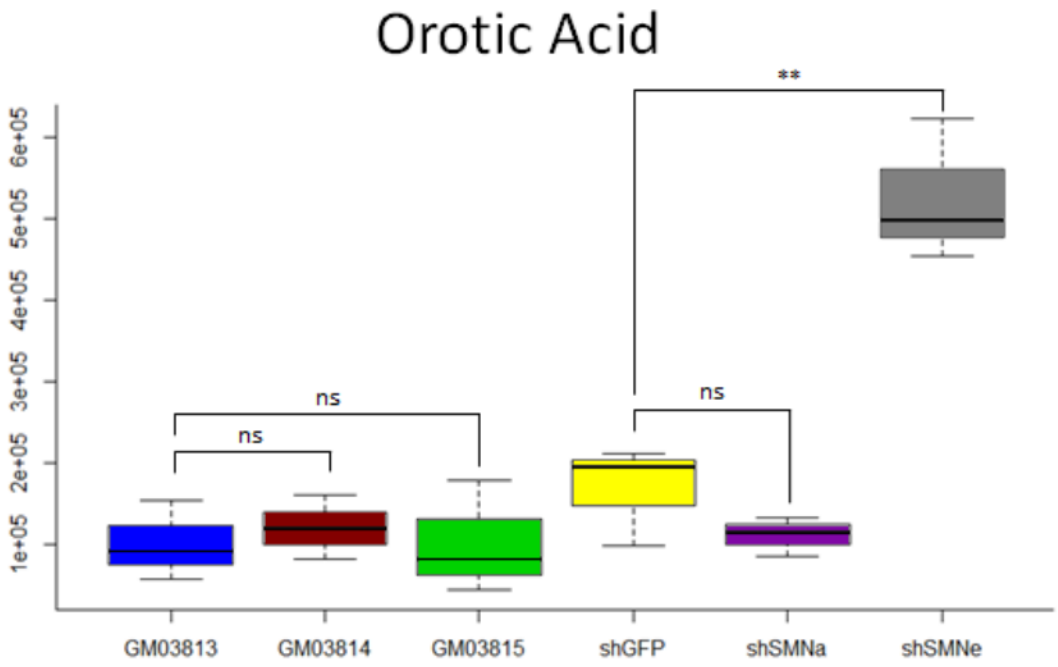

Supplementary Figure 1: Orotic acid is elevated in only GM03814 shSMNe. The accumulation of orotic acid in GM03814 shSMNe may explain why ROS is elevated in this SMN knockdown sample, yet not in GM03814 shSMNa.